LIUTEX AND STATISTICAL ANALYSIS FOR FLUID TRANSITION

by

Charles Matthew Nehemiah Nottage

Presented to the Faculty of the Graduate School of
The University of Texas at Arlington
in Partial Fulfillment of the Requirements for the
Degree of

Doctor of Philosophy

The University of Texas at Arlington
August 2021

DEDICATION

I want to dedicate this dissertation to my parents, Charles L. Nottage and Cassandra C. Nottage. You have been my strength when I was weak and my eyes when I could not see. You saw the best that was in me. You encouraged me when I started to second guess myself. You provided for me throughout my pursuit of this degree. Without you, I might not have made it this far. I love you both so much. Thank you for being my parents.

Acknowledgments

I would first like to give thanks to the Lord God Almighty for all the blessings, opportunities, protection, peace of mind, joy, knowledge, wisdom, and understanding during this journey to Ph.D. I know that he has brought me a mighty long way and has been with me every step of the way.

I would like to express my deep gratitude to my advisor Dr. Chaoqun Liu for his relentless guidance, support, and encouragement. I am thankful that he trusted me to complete this research project and be patient with me whenever I did not understand the task or misunderstood the process to get the results included in this thesis. His guidance and knowledge have helped me grow and mature into the academic researcher that I am today. I would also like to thank him for giving me the opportunity to participate in the 13th CHAOS 2020 conference as a presenter and a session chair. That experience was priceless and exposed me to new ideas and people.

Dr. Liu has helped me become a co-author of a few published journal papers and the first author of a few book chapters. Without him, I do not think it would have been possible to write such high-quality journals and conference papers. I am one of Dr. Liu's research team members, Center for Numerical Simulation and Modeling (CNSM) at the University of Texas at Arlington. I want to thank all my fellow researchers and friends at CNSM - Yifei Yu, Pushpa Shrestha, Oscar Alvarez, Dalal Almutairi, Vishwa Patel, Xuan My Trieu, and Aayush Bhattarai. I enjoyed every project and task that Dr. Liu assigned to me with the CNSM team. I am grateful for their support and the quality time they spent with me in problem-solving and research discussions.

I want to give a special thank you to Yifei Yu. Yifei Yu has worked on every paper that I am a co-author on, and he has always been very patient and understanding with me. Thank you so much for all the help with understanding the DNS Fortran codes. I would like to remember and thank my senior, Dr. Sita Chakrit. She will always have a place in my heart as my good friend. I am thankful for Ramesh Sharma, who helped me grow as a teacher by studying and discussing concepts with

me most of my time at UTA.

I am very thankful to Dr. Tuncay Aktosun for all the guidance, advice, and help along this journey. I am very thankful to Dr. Hristo Kojouharov, who introduced me to my love of Numerical Analysis when I took Scientific Computing with him. Dr. Kojouharov was always available to answer my questions about Numerical Analysis or anything related to being a graduate student. I am thankful to Dr. Jianzhong Su for giving me the opportunity to be a GTA, to graduate earlier than I expected, and the opportunity to be a postdoc fellow at UTA.

I want to thank my father, Charles L. Nottage, my mother, Cassandra C. Nottage, my sister Cassandra Nottage-Mackey and her husband Rajiv Mackey, and my grandmother Mary Nottage for all their support. I would also like to thank my brothers from other mothers Cleveland Wilson, Eronjha Adderley-Mcintosh, and Craig Cambridge, for being the brothers I always wanted. I would like to thank Jillian Braynen for always checking up on me and my progress.

I am thankful to all my high school and undergraduate Math Professors, who encouraged me to pursue a Ph.D. in mathematics. Thank you, Dr. Joseph Ferguson, Dr. Colin Ferreira, Dr. Yan Lyansky, Renate McWilliams, David McWilliams, and Dr. Janet Patterson-Curtis. Finally, I am thankful to everyone else who had some impact on my life during this time.

Abstract

LIUTEX AND STATISTICAL ANALYSIS FOR FLUID TRANSITION

Charles Matthew Nehemiah Nottage

The University of Texas at Arlington, 2021

Supervising Professor(s): Chaoqun Liu

A vortex can be intuitively recognized as the rotational swirling motion of the fluids. The fascination of this phenomenon brought about many years of research to define, classify, and identify the vortical structure. Throughout the decades, many vortex identification methods were developed and can be characterized into three generations. The generational methods are vorticity-based, eigenvalue-based such as Q, λ_{ci}, and λ_2, and Liutex-based. Before the development of Liutex, there was no mathematical definition for vortex.

Is Liutex superior to vorticity and the eigenvalue-based methods? Is the vorticity vector the local rotational axis? Should vorticity be considered vortex? In this dissertation, I answer these questions by utilizing dimensional analysis to examine and compare the eigenvalue-based methods with Liutex. Then, an analysis of vector candidates for the local rotational axis is conducted to identify which candidates satisfy the definition of the local rotational axis. Lastly, a statistical analysis of vorticity, Liutex, and shear is performed to show their behavior and relationship in the boundary layer from laminar flow to turbulent flow.

The results of these three procedures show that: Out of the four eigenvalue-based methods analyzed, λ_{ci} was the only one that was dimensionally consistent with Liutex. The Liutex directional vector was the only candidate that satisfied the definition of the local rotational axis, and vorticity should not be considered vortex as shear highly contaminates it.

Contents

List of Symbols

M_∞ = Mach number

Re = Reynolds number

x_{in} = distance between the leading edge of flat plate and upstream boundary of the computational domain

δ_{in} = inflow displacement thickness

Lx = length of the computational domain along the x-direction

Ly = length of the computational domain along the y-direction

Lz_{in} = height at the inflow boundary

T_w = wall temperature

T_∞ = free stream temperature

$*$ = multiplication operator

$\times$ = cross product

$\otimes$ = outer product

$\boldsymbol{\nabla}\vec{\mathbf{v}}$ = velocity gradient tensor

$\boldsymbol{\nabla}\overrightarrow{\boldsymbol{V}_\theta}$ = velocity gradient tensor in the principal coordinate

$\boldsymbol{A}_\theta$ = symmetric tensor in the principal coordinate

$\boldsymbol{B}_\theta$ = antisymmetric tensor in the principal coordinate

Q = Q criterion

Δ = Delta criterion

λ_{ci} = Lambda-ci criterion

λ_2 = Lambda-2 criterion

Ω = Omega criterion

$\overrightarrow{\omega}$ = vorticity vector

$\vec{R}$ = Liutex vector

R = Liutex magnitude

$\vec{r}$ = Directional vector of Liutex

α = angular velocity

l_{mag} = Liutex magnitude component

ω_{mag} = vorticity magnitude component

s_{mag} = shear magnitude component

l_y = Liutex component in the y direction

ω_y = vorticity component in the y direction

s_y = shear component in the y direction

Chapter 1
Introduction

A vortex is recognized as the rotational motion of fluids. Many vortex identification methods have been developed within the last several decades to track the vortical structure in a fluid flow; however, we still lacked unambiguous and universally accepted vortex identification criteria. This obstacle caused a lot of confusion and misunderstandings in turbulence research (Liu et al. 2014). In most research papers and textbooks, the vorticity tube/filament is regarded as vortex and the magnitude of the vorticity as the local rotational strength. Many researchers widely acknowledged the concept of vortex defined as the vorticity concentration and other vorticity-based methods (Helmholtz 1858, Saffman 1992) as the vorticity vector was believed to offer a mathematical definition of fluid rotational motion. The physics behind a vortex reveals that there exists a local fluid rotation axis. Many researchers and textbooks accept that the vorticity vector is the local fluid rotation axis. Zhou and Antonia utilized the spatially phased correlated vorticity to characterize large-scale and organized structures in the cylinder wake (Zhou & Antonia 1993). However, problems arose while applying in viscous flows, particularly in turbulent flows. The rigid rotation strength is smaller than the surrounding areas in turbulent viscous flows near the wall, where shear stress is dominant.

Many researchers in the literature have supported this claim, indicating the inadequacies of vorticity-based methods. Epps observed that vorticity could not distinguish a vortical region with rotational motions from a strong shear layer (Epps 2017). Robinson also uncovered that the regions of strong vorticity and actual vortices are weakly related (Robinson 1991). These vorticity-based methods are the first generation of vortex identification methods (Liu et al. 2019). To remedy the problems of vorticity-based methods, the second-generation vortex identification methods, which

are eigenvalue-based methods such as Δ (Perry 1987, Chong 1990), Q (Hunt et al. 1988), λ_2 (Jeong et al. 1995), λ_{ci} (Zhou et al. 1999), Ω (Liu et al. 2016, Dong et al. 2018), etc., have been introduced and extensively applied in visualizing vortex structures over the past four decades. Although these schemes can judge the presence of the local rotational motion to some extent, these methods require a threshold adjustment to visualize the iso-surface plot accurately.

This poses a problem because it is difficult to adjust to a proper threshold that will define the boundary of the vortical structures in a particular case (Liu et al. 2016, Zhang et al. 2018). Moreover, the Q and λ_2 methods are only workable for incompressible flows due to their incompressibility assumption. The issues of the first generation and second-generation vortex identification methods prompted the development of a new vortex identification method, the Liutex method (Liu et al. 2018, Gao et al. 2018), and the third-generation of vortex identification methods. Unlike the second-generation methods, the Liutex method is a novel eigenvector-based method that is local, accurate, unique, and systematic. Furthermore, the systematical definition of Liutex is given as a vector that has its corresponding scalar and tensor forms (Gao et al. 2018). The vector form of Liutex gives the direction of the local fluid rotation, while the magnitude of Liutex represents the rotational strength of a fluid rotation. Also, the Liutex vector is Galilean invariant (Haller 2005, Wang 2018, Liu et al. 2019). Correlation analysis between Liutex and the other vortex identification methods revealed that vorticity had the worst performance as its correlation was always weaker than the other methods (Yu et al. 2020, Yu et al. 2021).

This dissertation thesis proposes three questions: Is Liutex superior to vorticity and the eigenvalue-based methods? Is the vorticity vector the local rotational axis? Should vorticity be considered vortex? I answer these questions by utilizing dimensional analysis to examine and compare the eigenvalue-based methods with Liutex. Then, an analysis of vector candidates for the local rotational axis is conducted to identify which candidates satisfy the definition of the local rotational

axis. Lastly, a statistical analysis of vorticity, Liutex, and shear is performed to show their behavior and relationship in the boundary layer from laminar flow to turbulent flow.

The organization of this dissertation thesis is as follows: Chapter 2 introduces the Numerical data structure of the direct numerical simulation (DNS) used throughout the thesis. Chapter 3 gives a brief introduction to the vortex identification methods used in this dissertation. Chapter 4 introduces the principal coordinate system and principal decomposition utilized in chapters 5, 6, and 7. Chapter 5 covers the dimensional analysis of the second generational methods. Chapter 6 introduces the concept of the local fluid rotation axis and the possible candidates for it. Chapter 7 tackles the misunderstanding of vorticity being vortex.

Chapter 2
Numerical Data Structure

The research and results in this dissertation are computed using the direct numerical simulation (DNS) data of fluid flow in the flat plate boundary layer transition received from the Texas Advanced Computing Center (TACC) and are used to model and simulate the fluid flow. The Fortran code DNSUTA was developed by the Center for Numerical Simulation and Modeling (CNSM) at UTA under the leadership of Dr. Chaoqun Liu in 2009. The DNS code was also validated by NASA Langley. The results were compared to experiments and other DNS results (Wu et al. 2009, Yan et al. 2014). It was found to be consistent and accurate. The motion of a fluid can be described by the conservation of mass, momentum, and energy for an arbitrary control volume.

2.1 Governing Equations

2.1.1 Conservation of Mass (Continuity Equation)

Let S be a closed surface with volume V. S also has a fixed position with respect to the x, y, and z coordinates. Define ρ as the density of the fluid at a position (x, y, z) and at time t. Then, the mass of the fluid enclosed by the surface at any instance in time t is $\int \rho \mathrm{dV}$, and the net rate at which the mass flows outward across the surface is $\int \rho\vec{u} \cdot \hat{n}\, \mathrm{dS}$, where $\vec{u}$ is the velocity vector of mass flowing outwards across the surface, $\hat{n}$ is the unit normal vector directed outward from the surface S, dV is the infinitesimal volume, and dS is the closed surface area.

Note: volume = area × distance = dS × $\vec{u}t$.

According to the conservation of mass of the fluid, the net rate of fluid mass flowing is equal to the

net rate of fluid mass flowing outwards across the surface, i.e., $\frac{\partial}{\partial t}\int \rho \, \mathrm{dV} = -\int \rho\vec{u} \cdot \hat{n} \, \mathrm{dS}$. Since the volume V is fixed in space; the differentiation under the integral sign and the transformation of the surface integral (by the Gaussian divergence theorem) gives:

$$\int \frac{\partial \rho}{\partial t}\mathrm{dV} + \int \nabla \cdot (\rho\vec{u})\mathrm{dV} = 0 \text{ or, } \int \left[\frac{\partial \rho}{\partial t} + \nabla \cdot (\rho\vec{u})\right] \mathrm{dV} = 0. \quad (2.1)$$

This relation is valid for all V that lies entirely in the fluid, and therefore, it is continuous in x, y, and z. So, it must be identically zero everywhere in the fluid. Hence, the continuity equation is

$$\frac{\partial \rho}{\partial t} + \nabla \cdot (\rho\vec{u}) = 0. \quad (2.2)$$

Note: The Divergence theorem states that flux across the surface S is equal to the total divergence of $\vec{u}$ over the region that covers volume V, i.e., $\iint \rho\vec{u} \cdot \hat{n} \, \mathrm{dS} = \iiint \nabla \cdot \vec{u} \, \mathrm{dV}$.

2.1.2 Conservation of Momentum (Equation of Motion)

The conservation of momentum in a control volume V requires that the changes of momentum in this volume must be equal to what is gained/lost through the surface that encloses this volume and what is created/consumed by sources and sinks inside the control volume.

Similar to the continuity equation, consider a volume of fluid V enclosed by a surface S, fixed with respect to the coordinate axes. For this body of fluid, the momentum is given by the equation $\int \rho\vec{u} \, \mathrm{dV}$, and rate of change of momentum is given by,

$$\frac{\partial}{\partial t}\int \rho\vec{u} \, \mathrm{dV} = -\int \frac{\partial(\rho\vec{u})}{\partial t}\mathrm{dV}. \quad (2.3)$$

Now, the net rate of the gain or loss through the surface S is given by,

$$\int \rho\vec{u}(\vec{u} \cdot \hat{n}) \, \mathrm{dS} = \int \nabla \cdot (\rho\vec{u}\otimes\vec{u})\mathrm{dV}, \quad (2.4)$$

which is derived from the divergence theorem, i.e., the flux of a vector field through a closed surface is equal to the divergence of the field in the volume enclosed and $\otimes$ represents the

outer product, that is, $\rho\vec{u}\otimes\vec{u} = \rho\vec{u}\vec{u}^{\boldsymbol{T}}$ which is a tensor.

If we let $\boldsymbol{b}$ be the sources and sinks inside the control volume V, then the conservation of momentum inside the volume V is given by,

$$\int \frac{\partial(\rho\vec{u})}{\partial t}\mathrm{dV} = -\int \nabla\cdot(\rho\vec{u}\otimes\vec{u})\mathrm{dV} + \int \rho\boldsymbol{b}\ \mathrm{dV} \text{ or, } \int\left[\frac{\partial(\rho\vec{u})}{\partial t} + \nabla\cdot(\rho\vec{u}\otimes\vec{u}) - \rho\boldsymbol{b}\right]\mathrm{dV} = 0. \quad (2.5)$$

Since the volume V is arbitrary inside the fluid, then, $\frac{\partial(\rho\vec{u})}{\partial t} + \nabla\cdot(\rho\vec{u}\otimes\vec{u}) - \rho\boldsymbol{b} = 0$, where forces $\boldsymbol{b}$ can be separated into two types: the stress form forces and body forces.

Next, we have, $\rho\boldsymbol{b} = \rho\boldsymbol{f} + (\nabla\cdot\boldsymbol{\sigma})$ where $\boldsymbol{f}$ represents the body forces and $\boldsymbol{\sigma}$ is the stress force tensor. The stress force comprises the forces that act within a body to respond to externally applied forces and body forces. It can be divided into normal and shear components. If we assume a Newtonian fluid, there is a linear relation between the stress ($\boldsymbol{\sigma}$) and the rate of strain of the fluid, then by Stokes (1845), $\boldsymbol{\sigma} = -(p - \mu_v\nabla\cdot\vec{u})\mathbf{I} + \mu\left[\nabla\vec{u} + (\nabla\vec{u})^{\boldsymbol{T}} - \frac{2}{3}(\nabla\cdot\vec{u})\mathbf{I}\right]$, where p is the pressure, **I** is the identity matrix, μ_v is the bulk viscosity related to the viscosity μ, i.e.,

$\mu_\mathrm{v} = \lambda + \frac{2}{3}\mu$, and according to Stokes' hypothesis, μ is taken to make $\mu_\mathrm{v} = 0$. Therefore,

$$\boldsymbol{\sigma} = -p\mathbf{I} + \lambda(\nabla\cdot\vec{u})\mathbf{I} + \mu[\nabla\vec{u} + (\nabla\vec{u})^{\boldsymbol{T}}] = -\left[p + \frac{2}{3}\mu(\nabla\cdot\vec{u})\right]\mathbf{I} + \mu[\nabla\vec{u} + (\nabla\vec{u})^{\boldsymbol{T}}]. \quad (2.6)$$

Hence, the conservation of momentum equations can be written as:

$$\frac{\partial(\rho\vec{u})}{\partial t} + \nabla\cdot(\rho\vec{u}\otimes\vec{u}) = \rho\boldsymbol{f} - \nabla p - \frac{2}{3}\nabla[\mu(\nabla\cdot\vec{u})] + \nabla[\mu(\nabla\vec{u} + (\nabla\vec{u})^{\boldsymbol{T}})]. \quad (2.7)$$

2.1.3 Conservation of Energy

From the first law of thermodynamics, the conservation of energy for a fluid of volume V contained within a surface S can be found by calculating the work done on the mass of fluid by volume, surface forces, and the heat gained through transfer across the boundary and other sources inside the volume. The total energy E provides the conserved quantity and is defined as the sum of

its internal energy and kinetic energy per unit mass, i.e., $E = e + \frac{1}{2}\vec{u} \cdot \vec{u}$, where e is the internal energy per unit mass of the fluid.

The rate of change of the total energy inside the volume V contained within a surface S is $\frac{\partial}{\partial t}\int \rho E \, \mathrm{dV} = \int \frac{\partial(\rho E)}{\partial t} \mathrm{dV}$, while the net rate of what is gained or lost through the surface is

$$\int (\rho E)(\vec{u} \cdot \hat{n}) \, \mathrm{dS} = \int \nabla \cdot (\rho E)\vec{u} \, \mathrm{dV}. \quad (2.8)$$

Heat is also transferred to the fluid in the volume by molecular conduction through the surface S. Then, $\int (k\nabla T) \cdot \hat{n} \, \mathrm{dS} = \int \nabla \cdot (k\nabla T) \, \mathrm{dV}$, where T is the absolute temperature, and k is the thermal conductivity coefficient of the fluid. The work done on the fluid by forces can be divided into volume and surface sources.

The volume sources include the volume forces $\boldsymbol{f}$ and heat sources q_H other than conduction, such as radiation or heat released by chemical reactions. This gives the work done for the volume V,

$$\int (\rho \boldsymbol{f} \cdot \vec{u} + q_H) \, \mathrm{dV}. \quad (2.9)$$

The work done on the fluid by the surface sources, i.e., internal shear stresses ($\boldsymbol{\sigma}$) acting on the surface of the volume considering that there are no external surface heat sources, is given by, $\int (\boldsymbol{\sigma} \cdot \vec{u}) \cdot \hat{n} \, \mathrm{dS} = \int \nabla \cdot (\boldsymbol{\sigma} \cdot \vec{u}) \, \mathrm{dV}$. Grouping all terms, we get the energy conservation equation,

$\int \frac{\partial(\rho E)}{\partial t} \mathrm{dV} + \int \nabla \cdot (\rho E)\vec{u} \, \mathrm{dV} = \int \nabla \cdot (k\nabla T) \, \mathrm{dV} + \int (\rho \boldsymbol{f} \cdot \vec{u} + q_H) \, \mathrm{dV} + \int \nabla \cdot (\boldsymbol{\sigma} \cdot \vec{u}) \, \mathrm{dV}$, or

$\frac{\partial(\rho E)}{\partial t} + \nabla \cdot (\rho E)\vec{u} - \nabla \cdot (k\nabla T) - \nabla \cdot (\boldsymbol{\sigma} \cdot \vec{u}) = \rho \boldsymbol{f} \cdot \vec{u} + q_H$, and

$$\boldsymbol{\sigma} = -\left[p + \frac{2}{3}\mu(\nabla \cdot \vec{u})\right]\mathbf{I} + \mu[\nabla\vec{u} + (\nabla\vec{u})^{\boldsymbol{T}}]. \quad (2.10)$$

2.2. Numerical Setup

The computational domain has the grid number $1920 \times 128 \times 241$, representing the number of grids in streamwise (x), spanwise (y), and wall-normal (z) directions. In normal direction, these

grids are stretched, while in streamwise and spanwise directions, they are uniform. The length of the first grid interval in the normal direction at the entrance is 0.43 in wall units (Z+ = 0.43).

The flow parameters are listed in Table 2.1. Here, M_∞ is Mach number, Re is Reynolds number and, T_w and T_∞ are wall and free stream temperature, respectively. Likewise, x_{in} represents the distance between the leading edge and the inlet of the flat plate. Lx, Ly and Lz_{in} are the lengths of computational domain in x, y, and z directions. δ_{in} is the inflow displacement thickness.

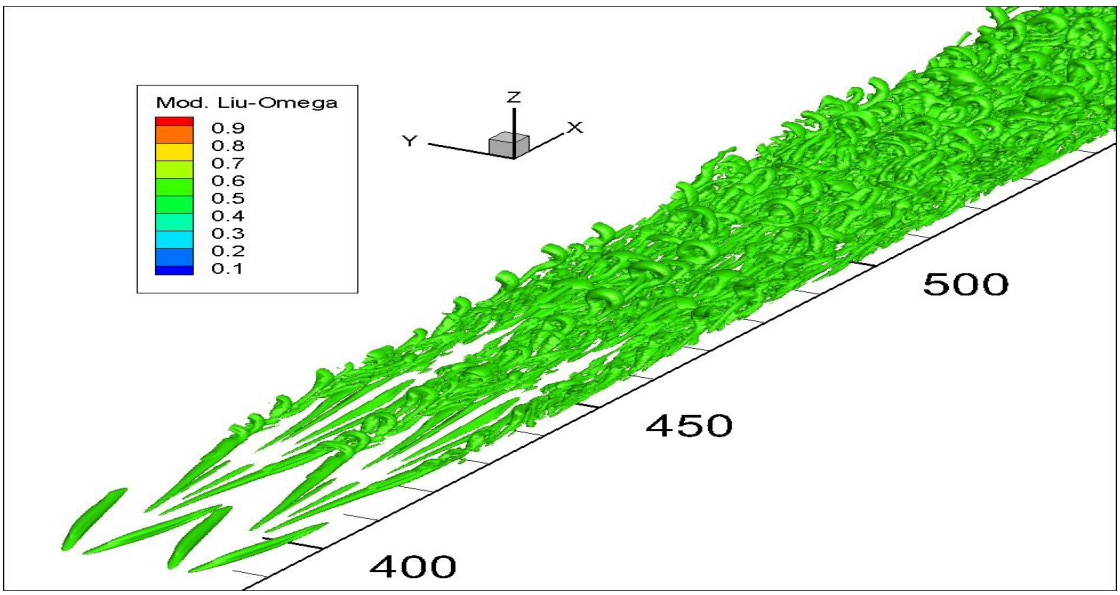

Figure 2.1. Vortex structure in transitional boundary with $\widetilde{\Omega}_L = 0.52$.

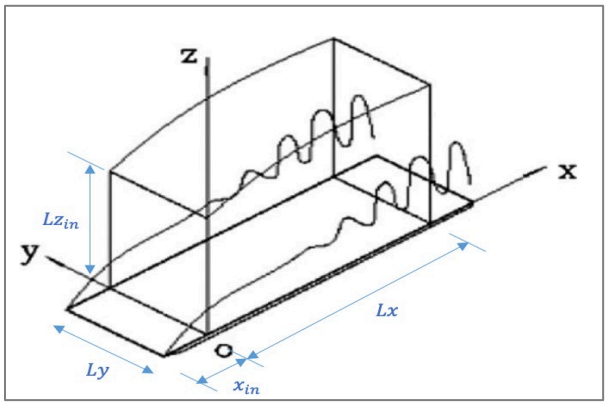

Figure 2.2. Computation domain

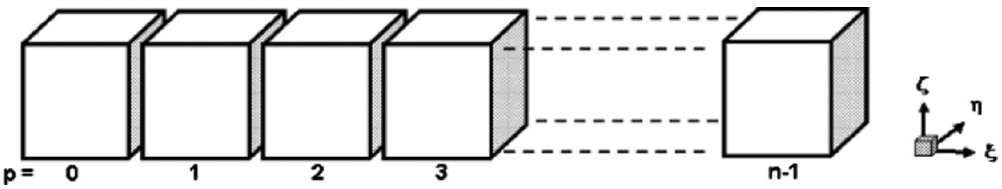

Figure 2.3. Domain decomposition along the streamwise direction in the computational space.

M_∞	Re	x_{in}	Lx	Ly	Lz_{in}	T_w	T_∞
0.5	1000	$300.79\delta_{in}$	$798.03\delta_{in}$	$22\delta_{in}$	$40\delta_{in}$	273.15K	273.15K

Table 2.1. DNS parameters

The parameters in Table 2.1 are defined as

M_∞ = Mach number

Re = Reynolds number

x_{in} = distance between the leading edge of flat plate and upstream boundary of the computational domain

δ_{in} = inflow displacement thickness

Lx = length of the computational domain along x direction

Ly = length of the computational domain along y direction

Lz_{in}= height at the inflow boundary

T_w = wall temperature

T_∞ = free stream temperature

For more details about case setup and validation of code, refer to Yan et al. 2014 and Liu et al. 2014. Other research papers such as Robinson 1991 and Wang et al. 2017 also use similar case setups.

Chapter 3

Vortex Identification Methods

The standard form of the velocity gradient tensor is:

$$\nabla\vec{\mathbf{v}} = \begin{bmatrix} \frac{\partial u}{\partial x} & \frac{\partial u}{\partial y} & \frac{\partial u}{\partial z} \\ \frac{\partial v}{\partial x} & \frac{\partial v}{\partial y} & \frac{\partial v}{\partial z} \\ \frac{\partial w}{\partial x} & \frac{\partial w}{\partial y} & \frac{\partial w}{\partial z} \end{bmatrix}.$$

3.1 First Generation: Vorticity

In 1858, Helmholtz introduced the concept of the vorticity tube/filament (Helmholtz 1858). Since then, many researchers have believed that vortices consist of small vorticity tubes called vortex filaments, and the magnitude of vorticity gives the vortex strength. The vorticity vector is mathematically defined as the curl of the velocity. i.e.,

$$\text{vorticity} = \nabla \times \vec{\mathbf{v}} = \begin{vmatrix} \mathbf{i} & \mathbf{j} & \mathbf{k} \\ \frac{\partial}{\partial x} & \frac{\partial}{\partial y} & \frac{\partial}{\partial z} \\ u & v & w \end{vmatrix} = \mathbf{i}\left(\frac{\partial w}{\partial y} - \frac{\partial v}{\partial z}\right) - \mathbf{j}\left(\frac{\partial w}{\partial x} - \frac{\partial u}{\partial z}\right) + \mathbf{k}\left(\frac{\partial v}{\partial x} - \frac{\partial u}{\partial y}\right). \quad (3.1)$$

Helmholtz also introduced vortex lines and vortex filaments based on the vorticity vector. These vortex lines are drawn through the fluid mass so that their direction at every point coincides with the direction of the momentary axis of rotation of the water particles lying in it. The vortex filament was defined as the portions of the fluid mass cut out by constructing corresponding vortex lines through all circumference points of an infinitely small surface element. This dissertation will define the vorticity tensor, vorticity vector in its vector form, and the vorticity magnitude below.

3.1.1 Vorticity Tensor

The vorticity tensor is the antisymmetric tensor $\boldsymbol{B}$ from the traditional Cauchy-Stokes decomposition of the velocity gradient tensor $\boldsymbol{\nabla}\vec{\mathbf{v}}$ (Liu et al. 2019):

$$\boldsymbol{B} = \frac{1}{2}(\boldsymbol{\nabla}\vec{\mathbf{v}} - \boldsymbol{\nabla}\vec{\mathbf{v}}^{\mathbf{T}}) = \begin{bmatrix} 0 & \frac{1}{2}\left(\frac{\partial u}{\partial y} - \frac{\partial v}{\partial x}\right) & \frac{1}{2}\left(\frac{\partial u}{\partial z} - \frac{\partial w}{\partial x}\right) \\ \frac{1}{2}\left(\frac{\partial v}{\partial x} - \frac{\partial u}{\partial y}\right) & 0 & \frac{1}{2}\left(\frac{\partial v}{\partial z} - \frac{\partial w}{\partial y}\right) \\ \frac{1}{2}\left(\frac{\partial w}{\partial x} - \frac{\partial u}{\partial z}\right) & \frac{1}{2}\left(\frac{\partial w}{\partial y} - \frac{\partial v}{\partial z}\right) & 0 \end{bmatrix}. \quad (3.2)$$

3.1.2 Vorticity Vector

The vorticity vector is derived as follows (Jeong 1995):

$$\vec{\omega} = \boldsymbol{\nabla} \times \vec{\mathbf{v}} = \left(\frac{\partial}{\partial x}, \frac{\partial}{\partial y}, \frac{\partial}{\partial z}\right)^{\boldsymbol{T}} \times (\mathrm{u}, \mathrm{v}, \mathrm{w})^{\boldsymbol{T}} = \left(\frac{\partial w}{\partial y} - \frac{\partial v}{\partial z}, \frac{\partial u}{\partial z} - \frac{\partial w}{\partial x}, \frac{\partial v}{\partial x} - \frac{\partial u}{\partial y}\right)^{\boldsymbol{T}}. \quad (3.3)$$

3.1.3 Vorticity Magnitude

The vorticity magnitude is defined as

$$\|\vec{\omega}\| = \sqrt{\left(\frac{\partial w}{\partial y} - \frac{\partial v}{\partial z}\right)^2 + \left(\frac{\partial u}{\partial z} - \frac{\partial w}{\partial x}\right)^2 + \left(\frac{\partial v}{\partial x} - \frac{\partial u}{\partial y}\right)^2}. \quad (3.4)$$

3.2 Second Generation: Eigenvalue-based Methods

3.2.1 Δ Method

The Δ method defines a vortex to be the region where the velocity gradient tensor $\boldsymbol{\nabla}\vec{\mathbf{v}}$ has one real eigenvalue and a pair of complex conjugate eigenvalues (Chong et al. 1990). If $\lambda_1,\ \lambda_2\ and\ \lambda_3$ are the eigenvalues of the 3× 3 matrix of $\boldsymbol{\nabla}\vec{\mathbf{v}}$, then the characteristic equation can be written as

$$\lambda^3 - tr(\boldsymbol{\nabla}\vec{\mathbf{v}})\lambda^2 - \frac{1}{2}[\mathrm{tr}(\boldsymbol{\nabla}\vec{\mathbf{v}}^2) - \mathrm{tr}(\boldsymbol{\nabla}\vec{\mathbf{v}})^2]\lambda - \det(\boldsymbol{\nabla}\vec{\mathbf{v}}) = \lambda^3 + D_1\lambda^2 + D_2\lambda + D_3 = 0. \quad (3.5)$$

D_1, D_2, and D_3 are the first, second, and third invariants and are given by:

$$D_1 = -(\lambda_1 + \lambda_2 + \lambda_3) = -tr(\vec{\mathbf{\nabla}}\vec{\mathbf{v}}), \tag{3.6}$$

$$D_2 = \lambda_1\lambda_2 + \lambda_2\lambda_3 + \lambda_3\lambda_1 = -\frac{1}{2}[tr(\vec{\mathbf{\nabla}}\vec{\mathbf{v}}^2) - tr(\vec{\mathbf{\nabla}}\vec{\mathbf{v}})^2], \tag{3.7}$$

$$D_3 = -\lambda_1\lambda_2\lambda_3 = -\det(\vec{\mathbf{\nabla}}\vec{\mathbf{v}}). \tag{3.8}$$

The discriminant of the characteristic equation of the velocity gradient tensor is given by:

$$\Delta = \left(\frac{\tilde{Q}}{3}\right)^3 + \left(\frac{\tilde{R}}{2}\right)^2, \tag{3.9}$$

where $\tilde{Q} = D_2 - \frac{1}{3}{D_1}^2$ and $\tilde{R} = D_3 + \frac{2}{27}\ {D_1}^3 - \frac{1}{3}D_1D_2$.

For incompressible flow, the first invariant $D_1 = 0$, which results in $\Delta = \left(\frac{D_2}{3}\right)^3 + \left(\frac{D_3}{2}\right)^2$. If $\Delta \leq 0$, this indicates that all three eigenvalues of $\vec{\mathbf{\nabla}}\vec{\mathbf{v}}$ are real, but if $\Delta > 0$, there exists one real and two conjugate complex eigenvalues, which means that the point is inside a vortex region. Although the Δ method can capture the vortex region successfully, it is susceptible to the threshold value, which is man-made and arbitrary in general.

3.2.2 Q Method

Proposed by Hunt, the Q method is one of the most popular methods used to visualize the vortex structure (Hunt et al. 1988). Q is defined as the difference between the squared Frobenius norms of the vorticity and strain-rate tensors. i.e.,

$$Q = \frac{1}{2}(\|\boldsymbol{B}\|_F^2 - \|\boldsymbol{A}\|_F^2). \tag{3.10}$$

$\boldsymbol{A}$ and $\boldsymbol{B}$ are the symmetric (strain-rate tensor) and antisymmetric (vorticity tensor) parts of the velocity gradient tensor from the traditional Cauchy-Stokes decomposition.

$$\boldsymbol{A} = \frac{1}{2}(\boldsymbol{\nabla}\vec{\mathbf{v}} + \boldsymbol{\nabla}\vec{\mathbf{v}}^{\boldsymbol{T}}) = \begin{bmatrix} \frac{\partial u}{\partial x} & \frac{1}{2}\left(\frac{\partial u}{\partial y} + \frac{\partial v}{\partial x}\right) & \frac{1}{2}\left(\frac{\partial u}{\partial z} + \frac{\partial w}{\partial x}\right) \\ \frac{1}{2}\left(\frac{\partial v}{\partial x} + \frac{\partial u}{\partial y}\right) & \frac{\partial v}{\partial y} & \frac{1}{2}\left(\frac{\partial v}{\partial z} + \frac{\partial w}{\partial y}\right) \\ \frac{1}{2}\left(\frac{\partial w}{\partial x} + \frac{\partial u}{\partial z}\right) & \frac{1}{2}\left(\frac{\partial w}{\partial y} + \frac{\partial v}{\partial z}\right) & \frac{\partial w}{\partial z} \end{bmatrix} \tag{3.11}$$

$$\boldsymbol{B} = \frac{1}{2}(\boldsymbol{\nabla}\vec{\mathbf{v}} - \boldsymbol{\nabla}\vec{\mathbf{v}}^{\boldsymbol{T}}) = \begin{bmatrix} 0 & \frac{1}{2}\left(\frac{\partial u}{\partial y} - \frac{\partial v}{\partial x}\right) & \frac{1}{2}\left(\frac{\partial u}{\partial z} - \frac{\partial w}{\partial x}\right) \\ \frac{1}{2}\left(\frac{\partial v}{\partial x} - \frac{\partial u}{\partial y}\right) & 0 & \frac{1}{2}\left(\frac{\partial v}{\partial z} - \frac{\partial w}{\partial y}\right) \\ \frac{1}{2}\left(\frac{\partial w}{\partial x} - \frac{\partial u}{\partial z}\right) & \frac{1}{2}\left(\frac{\partial w}{\partial y} - \frac{\partial v}{\partial z}\right) & 0 \end{bmatrix} \tag{3.12}$$

The Q method considers that a vortex occurs in the region where $Q > 0$. The Q method is currently the most popular method used in research. However, Q is scalar-valued, and a proper threshold is required to visualize the vortex region, which is kind of arbitrarily chosen.

3.2.3 λ_2 Method

The λ_2 criterion is calculated based on the observation that pressure tends to be the lowest on the axis of a swirling motion of fluid particles in a vortical region. This occurs because the centrifugal force is balanced by the pressure force (the cyclostrophic balance). This method is valid only in a steady inviscid planar flow (Jeong et al. 1995). However, this assumption fails to accurately identify vortices under strong, unsteady, and viscous conditions. By neglecting these unsteady and viscous effects, the symmetric part $\boldsymbol{S}$ of the gradient of the incompressible Navier–Stokes equation can be expressed as $\boldsymbol{S} = \boldsymbol{A}^2 + \boldsymbol{B}^2 = -\frac{\boldsymbol{\nabla}(\boldsymbol{\nabla}p)}{\rho}$, where p is pressure, ρ is density and $\boldsymbol{S}$ is a representation of the pressure Hessian matrix, i.e., $((\boldsymbol{\nabla}(\boldsymbol{\nabla}p))_{ij} = \frac{\partial^2 p}{\partial x_i \partial y_i}$.

Jeong and Hussain (Jeong et al. 1995) defined the vortex core as a connected region with two positive eigenvalues of the pressure Hessian matrix, i.e., a connected region with two negative eigenvalues of the symmetric tensor $\boldsymbol{S}$. If λ_1, λ_2 & λ_3 are three real eigenvalues of the symmetric

tensor $\boldsymbol{S}$, then by reordering them as $\lambda_1 \geq \lambda_2 \geq \lambda_3$, there must be $\lambda_2 < 0$ as two eigenvalues are negative, which confirms the existence of a vortex. In general, λ_2 cannot be expressed in terms of eigenvalues of the velocity gradient tensor; however, in some special cases, when eigenvectors are orthonormal, λ_2 can be exclusively determined by eigenvalues of the velocity gradient tensor. The vortex structure can be visualized as iso-surface by selecting a proper threshold of λ_2 (Liu et al. 2019).

3.2.4 $\boldsymbol{\lambda_{ci}}$ Method

The λ_{ci} criterion (Zhou et al. 1999, Chakraborty et al. 2005) uses the imaginary part of the velocity gradient tensor's complex eigenvalues to visualize the vortex structure. It is based on the idea that the local time-frozen streamlines exhibit a rotational flow pattern when $\boldsymbol{\nabla}\vec{\mathbf{v}}$ has a pair of complex conjugate eigenvalues. In this case, the tensor transformation of $\boldsymbol{\nabla}\vec{\mathbf{v}}$ is given by:

$\boldsymbol{\nabla}\vec{\mathbf{v}} = [\vec{v}_r\ \vec{v}_{cr}\ \vec{v}_{ci}]\begin{bmatrix}\lambda_r & 0 & 0\\ 0 & \lambda_{cr} & \lambda_{ci}\\ 0 & -\lambda_{ci} & \lambda_{cr}\end{bmatrix}[\vec{v}_r\ \vec{v}_{cr}\ \vec{v}_{ci}]^{-1}$, where λ_r is the real eigenvalue with the corresponding eigenvector $\vec{v}_r$ and the pair of complex conjugate eigenvalues are $\lambda_{cr} \pm i\lambda_{ci}$ with corresponding eigenvectors $\vec{v}_{cr} \pm i\,\vec{v}_{ci}$. In this case, in the local curvilinear system (c_1, c_2, c_3) spanned by the eigenvector $(\vec{v}_r, \vec{v}_{cr}, \vec{v}_{ci})$, the instantaneous streamlines exhibit a spiral motion. The equations of such streamlines can be written as:

$$c_1(t) = c_1(0)e^{\lambda_r t}\ , \tag{3.13}$$

$$c_2(t) = [c_2(0)\cos(\lambda_{ci}t) + c_3(0)sin(\lambda_{ci}t)]e^{\lambda_{cr}t}\ , \tag{3.14}$$

$$c_3(t) = [c_3(0)\cos(\lambda_{ci}t) - c_2(0)sin(\lambda_{ci}t)]e^{\lambda_{cr}t}\ , \tag{3.15}$$

where t represents the time parameter and constants $c_1(0)$, $c_2(0)$, and $c_3(0)$ are determined by initial conditions (Liu et al. 2019).

3.2.5 Ω Method

The Omega method originated from an important physical understanding that a vortex is a region where the vorticity overtakes the deformation. The vorticity cannot directly represent the fluid rotation, although there is no rigid rotation without vorticity. Therefore, the vorticity could be small in the region with strong rotation and large in the region with weak or zero rotation. The Blasius boundary layer is a typical example. The deformation is also an essential factor in a rotational flow while a vortex presents. Therefore, it is reasonable to consider the ratio of vorticity and the deformation for vortex identification. As given in Ref. (Liu et al. 2016), Ω is defined as the ratio of the vorticity tensor norm squared over the sum of the vorticity tensor norm squared and deformation tensor norm squared, i.e.,

$$\Omega = \frac{\|B\|_F^2}{\|A\|_F^2+\|B\|_F^2} = \frac{b}{a+b}. \tag{3.16}$$

In practice, a small positive parameter ε is added to the denominator of Ω to avoid non-physical noises so that Ω can be expressed as $\Omega = \frac{b}{a+b+\varepsilon}$ and $\varepsilon = 0.001 \times (b-a)_{max}$ (Dong et al. 2018). The $(b-a)_{max}$ term represents the maximum of the difference of the vorticity squared and the deformation squared. This term is easy to obtain at each timestep in a certain case. This allows us to avoid manually adjusting ε in many cases. The Omega method requires a parameter larger than 0.5 as the threshold. In practice, Ω = 0.51 or Ω = 0.52 can be used as the fixed threshold because the omega method is threshold insensitive.

3.3 Third Generation: Liutex-based Method

3.3.1 Liutex Method

Liutex (Liu et al. 2018, Gao and Liu 2018) is a vector defined as $\vec{R} = R\vec{r}$. R represents the Liutex magnitude defined as twice the angular velocity, and $\vec{r}$ represents the directional unit vector of Liutex. According to Wang (Wang et al. 2019), $\vec{r}$ is the real eigenvector of the velocity gradient tensor, and the explicit formula of R is

$$R = \vec{\omega} \cdot \vec{r} - \sqrt{(\vec{\omega} \cdot \vec{r})^2 - 4\lambda_{ci}^2} \,. \tag{3.17}$$

Liutex, as a vector, overcomes the drawbacks of the scalar methods, e.g., the threshold requirement when creating and analyzing graphics.

Chapter 4

Principal Coordinate System

4.1 Principal Coordinate

We have that $\boldsymbol{\nabla\vec{v}} = \begin{bmatrix} \frac{\partial u}{\partial x} & \frac{\partial u}{\partial y} & \frac{\partial u}{\partial z} \\ \frac{\partial v}{\partial x} & \frac{\partial v}{\partial y} & \frac{\partial v}{\partial z} \\ \frac{\partial w}{\partial x} & \frac{\partial w}{\partial y} & \frac{\partial w}{\partial z} \end{bmatrix}$, let $\mathbf{Q}$ be an orthogonal matrix that rotates the xyz frame to XYZ frame so that the Z-axis is parallel with the real eigenvector $\vec{r}$ of $\boldsymbol{\nabla\vec{v}}$. In general,

$\boldsymbol{\nabla\vec{V}} = \mathbf{Q}\boldsymbol{\nabla\vec{v}}\mathbf{Q}^{\boldsymbol{T}} = \begin{bmatrix} \frac{\partial U}{\partial X} & \frac{\partial U}{\partial Y} & 0 \\ \frac{\partial V}{\partial X} & \frac{\partial V}{\partial Y} & 0 \\ \frac{\partial W}{\partial X} & \frac{\partial W}{\partial Y} & \frac{\partial W}{\partial Z} \end{bmatrix}$. Define $\boldsymbol{P} = \begin{bmatrix} cos\theta & sin\theta & 0 \\ -sin\theta & cos\theta & 0 \\ 0 & 0 & 1 \end{bmatrix}$ the rotation matrix around the fixed Z-axis. Next, rotating through θ around the Z-axis will give you the Principal Coordinates XY plane (Yu et al. 2020).

$$\overrightarrow{\boldsymbol{\nabla V}_{\theta}} = \boldsymbol{P}\boldsymbol{\nabla\vec{V}}\boldsymbol{P^T} = \begin{bmatrix} \lambda_{cr} & \frac{\partial U}{\partial Y} & 0 \\ \frac{\partial V}{\partial X} & \lambda_{cr} & 0 \\ \frac{\partial W}{\partial X} & \frac{\partial W}{\partial Y} & \lambda_r \end{bmatrix} = \begin{bmatrix} \lambda_{cr} & -\frac{1}{2}R & 0 \\ \frac{1}{2}R + \varepsilon & \lambda_{cr} & 0 \\ \xi & \eta & \lambda_r \end{bmatrix}, \tag{4.1}$$

where $\frac{\partial \mathrm{U}}{\partial \mathrm{Y}} < 0$ and $\left|\frac{\partial \mathrm{U}}{\partial \mathrm{Y}}\right| \leq \left|\frac{\partial \mathrm{V}}{\partial \mathrm{X}}\right|$.

4.2 Principal Decomposition

$$\nabla\overrightarrow{\boldsymbol{V}_\theta} = \begin{bmatrix} \lambda_{cr} & -\frac{1}{2}R & 0 \\ \frac{1}{2}R+\varepsilon & \lambda_{cr} & 0 \\ \xi & \eta & \lambda_r \end{bmatrix} = \begin{bmatrix} 0 & -\frac{R}{2} & 0 \\ \frac{R}{2} & 0 & 0 \\ 0 & 0 & 0 \end{bmatrix} + \begin{bmatrix} 0 & 0 & 0 \\ \varepsilon & 0 & 0 \\ \xi & \eta & 0 \end{bmatrix} + \begin{bmatrix} \lambda_{cr} & 0 & 0 \\ 0 & \lambda_{cr} & 0 \\ 0 & 0 & \lambda_r \end{bmatrix} = \boldsymbol{R}+\boldsymbol{S}+\boldsymbol{C} \tag{4.2}$$

$\boldsymbol{R}$, $\boldsymbol{S}$, and $\boldsymbol{C}$ represent the rotation part, the shear part, and the stretching part, respectfully. This decomposition is unique and Galilean invariant (Yu et al. 2020).

Chapter 5
Dimensional Analysis

The dimension of any physical quantity expresses its dependence on the base quantities as a product of symbols (or powers of symbols) representing the base quantities. The importance of dimension arises from the fact that any mathematical equation relating physical quantities must be dimensionally consistent. (Moebs et al. 2016)

Base Quantity	Symbol for Dimension
Length	L
Mass	M
Time	T
Temperature	Θ

Table 5.1: List of the Base quantities and corresponding Dimension Symbols.

The Dimension of α is $\frac{1}{T}$ or T^{-1}. Liutex magnitude R is defined as twice the angular velocity, i.e., $R = 2\alpha$. This implies that Liutex magnitude R has the same dimension as angular velocity α. Therefore, these two quantities are relatable because their dimensions are consistent. We will focus on the R components of the following 2nd generation methods and analyze their dimensional consistency with α. (Nottage et al. 2021)

5.1 Mathematical Calculation

5.1.1 Δ Method

Recall:

$$\nabla\overrightarrow{V_\theta} = \begin{bmatrix} \lambda_{cr} & -\frac{1}{2}R & 0 \\ \frac{1}{2}R + \varepsilon & \lambda_{cr} & 0 \\ \xi & \eta & \lambda_r \end{bmatrix}.$$

The characteristic equation of velocity gradient tensor $\nabla\overrightarrow{V_\theta}$ is:

$$(\lambda - \lambda_r)\left[(\lambda - \lambda_{cr})^2 + \frac{R}{2}\left(\frac{R}{2} + \varepsilon\right)\right] = 0. \tag{5.1}$$

This implies that the three eigenvalues are:

$$\lambda_1 = \lambda_r, \qquad \lambda_2 = \lambda_{cr} + i\sqrt{\frac{R}{2}\left(\frac{R}{2} + \varepsilon\right)}, \qquad \lambda_3 = \lambda_{cr} - i\sqrt{\frac{R}{2}\left(\frac{R}{2} + \varepsilon\right)}$$

$$D_1 = -(\lambda_1 + \lambda_2 + \lambda_3) = -\lambda_r - 2\lambda_{cr}\,, \tag{5.2}$$

$$D_2 = \lambda_1\lambda_2 + \lambda_2\lambda_3 + \lambda_3\lambda_1 = 2\lambda_r\lambda_{cr} + \lambda_{cr}^2 + \frac{R}{2}\left(\frac{R}{2} + \varepsilon\right), \tag{5.3}$$

$$D_3 = -\lambda_1\lambda_2\lambda_3 = -\lambda_r\left[\lambda_{cr}^2 + \frac{R}{2}\left(\frac{R}{2} + \varepsilon\right)\right] \tag{5.4}$$

$$\tilde{Q} = D_2 - \frac{1}{3}{D_1}^2 = -\frac{1}{3}(\lambda_{cr} - \lambda_r)^2 + \frac{R}{2}\left(\frac{R}{2} + \varepsilon\right) \tag{5.5}$$

$$\tilde{R} = D_3 + \frac{2}{27}{D_1}^3 - \frac{1}{3}D_1D_2 = \frac{2}{27}(\lambda_{cr} - \lambda_r)^3 + \frac{2}{3}(\lambda_{cr} - \lambda_r)\frac{R}{2}\left(\frac{R}{2} + \varepsilon\right) \tag{5.6}$$

Then, the expression for Δ can be written as:

$$\Delta = \left(\frac{\tilde{Q}}{3}\right)^3 + \left(\frac{\tilde{R}}{2}\right)^2$$

$$= \frac{1}{243}\left[9\left(\frac{R}{2}\right)^3\left(\frac{R}{2} + \varepsilon\right)^3 - 6\left(\frac{R}{2}\right)^2\left(\frac{R}{2} + \varepsilon\right)^2(\lambda_{cr} - \lambda_r)^2 + \frac{5R}{2}\left(\frac{R}{2} + \varepsilon\right)(\lambda_{cr} - \lambda_r)^4\right] \tag{5.7}$$

The highest power of R present in Δ is R^6. Therefore, the dimension of Δ is equivalent to the dimension of α^6, which is T^{-6}. Since the dimension of angular velocity α is T^{-1}, Δ is not dimensionally consistent with α. (Nottage et al. 2021)

5.1.2 Q Method

Recall:

$$\boldsymbol{A}_\theta = \begin{bmatrix} \frac{\partial U}{\partial X} & \frac{1}{2}\left(\frac{\partial U}{\partial Y}+\frac{\partial V}{\partial X}\right) & \frac{1}{2}\left(\frac{\partial U}{\partial Z}+\frac{\partial W}{\partial X}\right) \\ \frac{1}{2}\left(\frac{\partial V}{\partial X}+\frac{\partial U}{\partial Y}\right) & \frac{\partial V}{\partial Y} & \frac{1}{2}\left(\frac{\partial V}{\partial Z}+\frac{\partial W}{\partial Y}\right) \\ \frac{1}{2}\left(\frac{\partial W}{\partial X}+\frac{\partial U}{\partial Z}\right) & \frac{1}{2}\left(\frac{\partial W}{\partial Y}+\frac{\partial V}{\partial Z}\right) & \frac{\partial W}{\partial Z} \end{bmatrix} = \begin{bmatrix} \lambda_{cr} & \frac{\varepsilon}{2} & \frac{\xi}{2} \\ \frac{\varepsilon}{2} & \lambda_{cr} & \frac{\eta}{2} \\ \frac{\xi}{2} & \frac{\eta}{2} & \lambda_r \end{bmatrix} \tag{5.8}$$

$$\boldsymbol{B}_\theta = \begin{bmatrix} 0 & \frac{1}{2}\left(\frac{\partial U}{\partial Y}-\frac{\partial V}{\partial X}\right) & \frac{1}{2}\left(\frac{\partial U}{\partial Z}-\frac{\partial W}{\partial X}\right) \\ \frac{1}{2}\left(\frac{\partial V}{\partial X}-\frac{\partial U}{\partial Y}\right) & 0 & \frac{1}{2}\left(\frac{\partial V}{\partial Z}-\frac{\partial W}{\partial Y}\right) \\ \frac{1}{2}\left(\frac{\partial W}{\partial X}-\frac{\partial U}{\partial Z}\right) & \frac{1}{2}\left(\frac{\partial W}{\partial Y}-\frac{\partial V}{\partial Z}\right) & 0 \end{bmatrix} = \begin{bmatrix} 0 & -\frac{R+\varepsilon}{2} & -\frac{\xi}{2} \\ \frac{R+\varepsilon}{2} & 0 & -\frac{\eta}{2} \\ \frac{\xi}{2} & \frac{\eta}{2} & 0 \end{bmatrix} \tag{5.9}$$

Then, $Q = \frac{1}{2}(\|\boldsymbol{B}_\theta\|_F^2 - \|\boldsymbol{A}_\theta\|_F^2)$

$$= \frac{1}{2}\left[2\left(\frac{R}{2}+\frac{\varepsilon}{2}\right)+2\left(\frac{\xi}{2}\right)^2+2\left(\frac{\eta}{2}\right)^2\right] - \frac{1}{2}\left[2\,{\lambda_{cr}}^2+{\lambda_r}^2+2\left(\frac{\varepsilon}{2}\right)^2+2\left(\frac{\xi}{2}\right)^2+2\left(\frac{\eta}{2}\right)^2\right]$$

$$= \left(\frac{R}{2}\right)^2 + \frac{1}{2}R\varepsilon - {\lambda_{cr}}^2 - \frac{1}{2}{\lambda_r}^2 \,. \tag{5.10}$$

The highest power of R present in Q is R^2. Therefore, the dimension of Q is equivalent to the dimension of α^2, which is T^{-2}. Since the dimension of angular velocity α is T^{-1}, Q is not dimensionally consistent with α. (Nottage et al. 2021)

5.1.3 λ_{ci} Method

Recall from 5.1.1, the eigenvalues of velocity gradient tensor $\boldsymbol{\nabla}\overrightarrow{\boldsymbol{V}_\theta}$ are:

$$\lambda_1 = \lambda_r, \qquad \lambda_2 = \lambda_{cr} + i\sqrt{\frac{R}{2}\left(\frac{R}{2}+\varepsilon\right)}, \qquad \lambda_3 = \lambda_{cr} - i\sqrt{\frac{R}{2}\left(\frac{R}{2}+\varepsilon\right)}\,.$$

Since rotation is orthogonal, the eigenvalues are the same as the original velocity gradient tensor, i.e., $\lambda_2 = \lambda_{cr} + i\lambda_{ci}$ and $\lambda_3 = \lambda_{cr} - i\lambda_{ci}$.

This implies that, $\lambda_{ci} = \sqrt{\frac{R}{2}\left(\frac{R}{2}+\varepsilon\right)}$. (5.11)

The highest power of R present in λ_{ci} is R^1. Therefore, the dimension of λ_{ci} is equivalent to the dimension of α, which is T^{-1}. Which implies that λ_{ci} is dimensionally consistent with α. (Nottage et al. 2021)

5.2 Graphical Representation

Two graphical examples are considered and analyzed to illustrate the importance of the dimensional quantifier of the methods.

5.2.1 2D Rigid Rotation

Consider 2D rigid rotation (Gao et al. 2018). The velocity in polar coordinates and cartesian coordinates are expressed as:

$$\begin{cases} v_r = \alpha r \\ v_\theta = 0 \end{cases}, \quad \begin{cases} u = -\alpha y \\ v = \alpha x \end{cases},$$

where α represents the angular velocity, which is a positive constant.

The velocity gradient tensor for this example is $\boldsymbol{\nabla}\overrightarrow{\boldsymbol{V}_\theta} = \begin{bmatrix} 0 & -\alpha & 0 \\ \alpha & 0 & 0 \\ 0 & 0 & 0 \end{bmatrix}$.

Recall: $\alpha = \frac{R}{2}$.

We can analytically express the second-generation methods as:

$\Delta = \frac{1}{27}\alpha^6$, $Q = \alpha^2$, $-\lambda_2 = \alpha^2$, and $\lambda_{ci} = \alpha$.

The value of α is increased by increments of 0.2, and the flow of the values is depicted in Fig. 5.1.

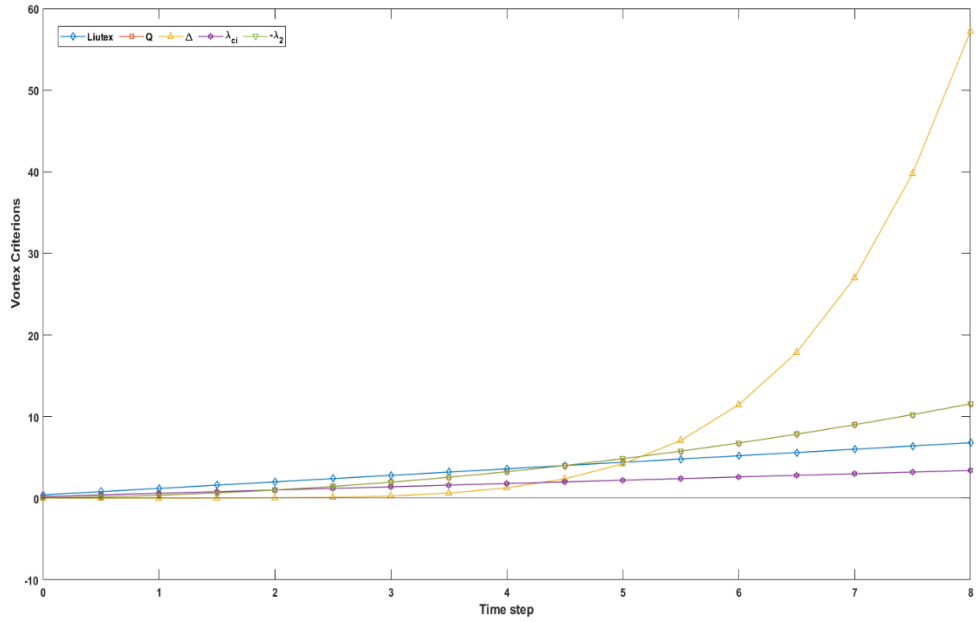

Fig. 5.1: Line graphs depicting the values of the Criterions with respect to α with a 0.2 increase on α at each time step.

In Fig. 5.1, λ_{ci} is the best second-generation method when compared to Liutex, which is considered as the exact quantity of rotation, because in 2D rigid rotation λ_{ci} is equal to the angular velocity α. On the other hand, as α increases, the values of the other criteria spread out further away from the value of α. Q and $-\lambda_2$ increase similarly from α since both have dimension T^{-2}. While Δ increases in value significantly from α. This occurs because the dimension of Δ is T^{-6}. The increment is so different from the other methods that Δ is the most inaccurate in terms of quantifying the value of the angular velocity α.

5.2.2 Boundary Layer Transition DNS

A DNS simulation of boundary transition of which the grid level is $1920 \times 128 \times 241$ is conducted. Three X positions are chosen from the grid, namely 402.8, 500.7, and 815.5. These positions are chosen from the laminar, transitional, and turbulent flow, respectively. Liutex

magnitude R is used in comparison with the values of the other methods since it is twice the angular velocity α. (Nottage et al. 2021)

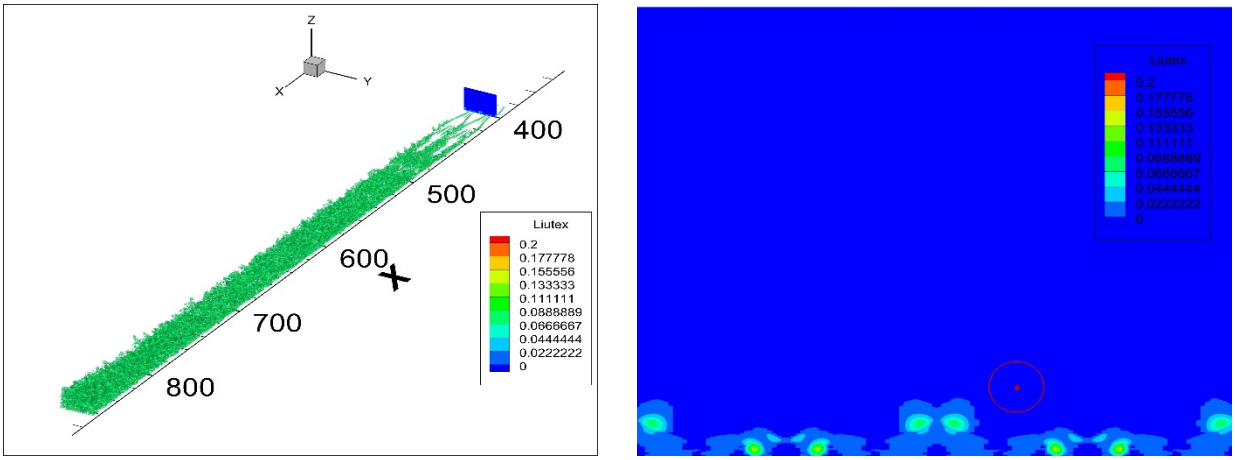

Fig 5.2: The point selected in Laminar Flow at x=402.8

Laminar flow is the area at the beginning of the vortex structure, where the vortex starts to develop. If there is vortex activity in this area, the strength of the vortex should be minimal and close to 0. Fig. 5.2 shows that this area's vortical structure is symmetrical.

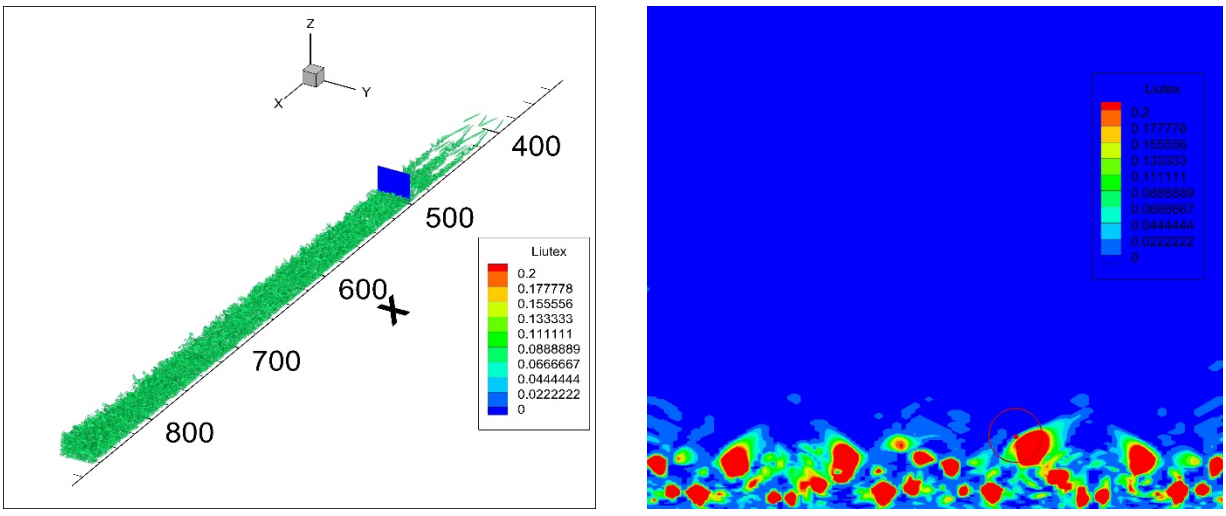

Fig. 5.3: The point selected in Transitional Flow at x=500.7

Transitional flow is where the vortex strength begins to increase, and the formation of hairpin vortex rings begins to appear. Fig. 5.3 shows that this area's vortical structure is mostly

symmetrical.

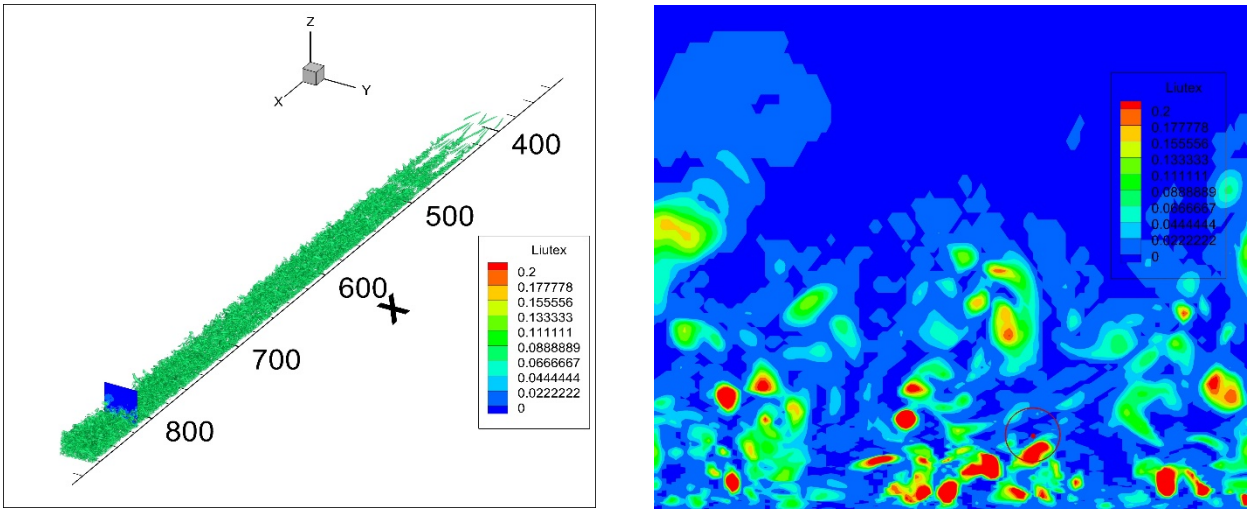

Fig. 5.4: The point selected in turbulent flow at x=815.5

Turbulent flow is where many hairpin vortex rings have formed, and the strength of the vortex varies between strong and weak. Fig. 5.4 shows that this area is very chaotic and antisymmetric.

One hundred snapshots of the data were observed and recorded. The relative values are computed to get a better comparison between the data values of the methods. The relative data values are derived by dividing the original data values by the absolute value of the max data value for each method. i.e., $\frac{data_{ni}}{\left|\max_{1\leq m\leq 100}(data_{mi})\right|} = RD_{ni}$, where $data$ represents the original data value, RD represents the relative data value, n = 1 to 100 and $i \in \{Q,\ \Delta, \lambda_2, \lambda_{ci},\ Liutex\}$. The data and relative data values are depicted in the following graphs.

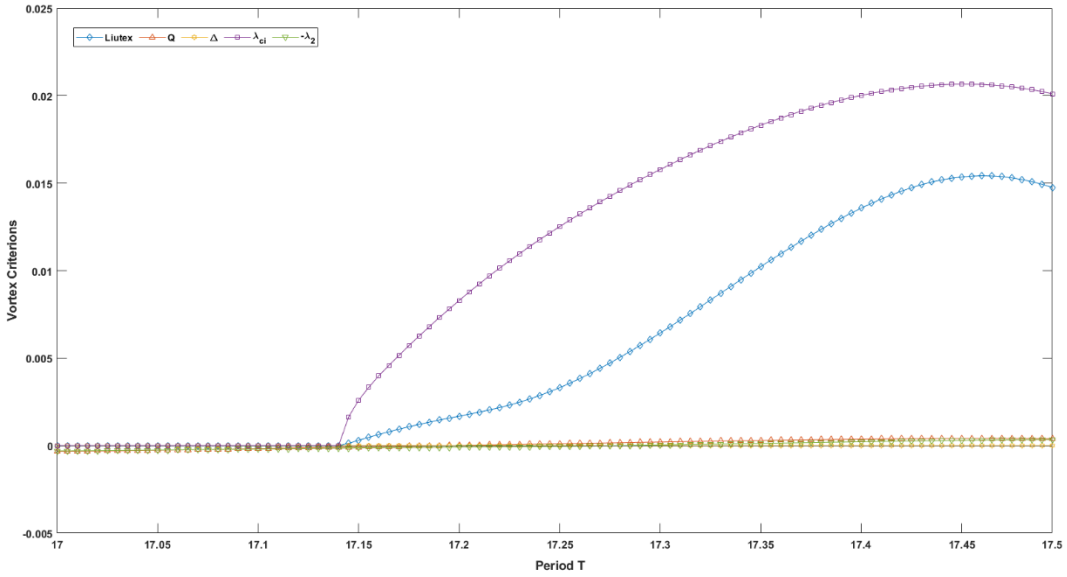

Fig. 5.5: Values of vortex criteria in different period T at x=402.8

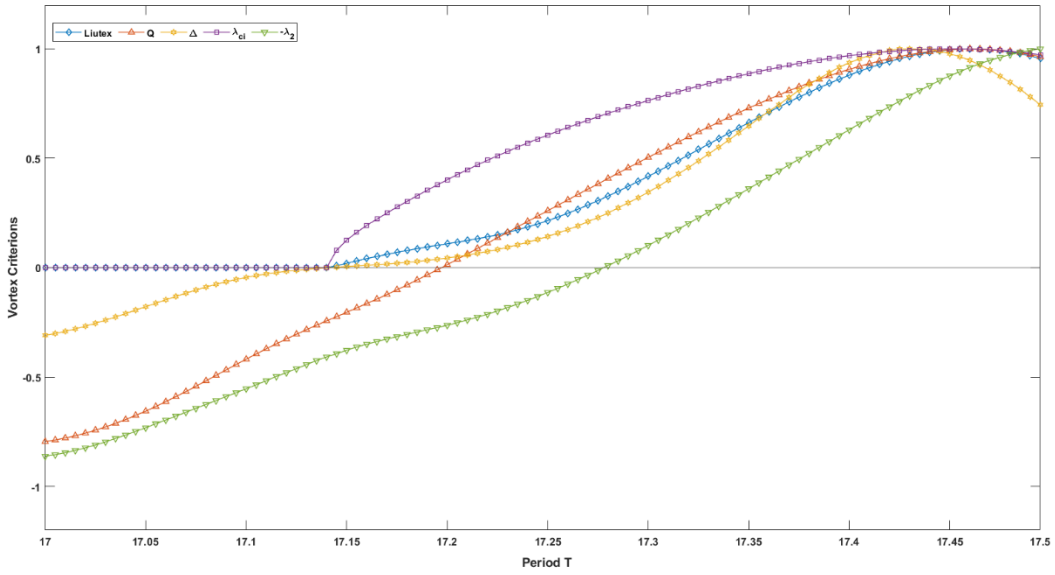

Fig. 5.6: Relative values of vortex criteria in different period T at x=402.8

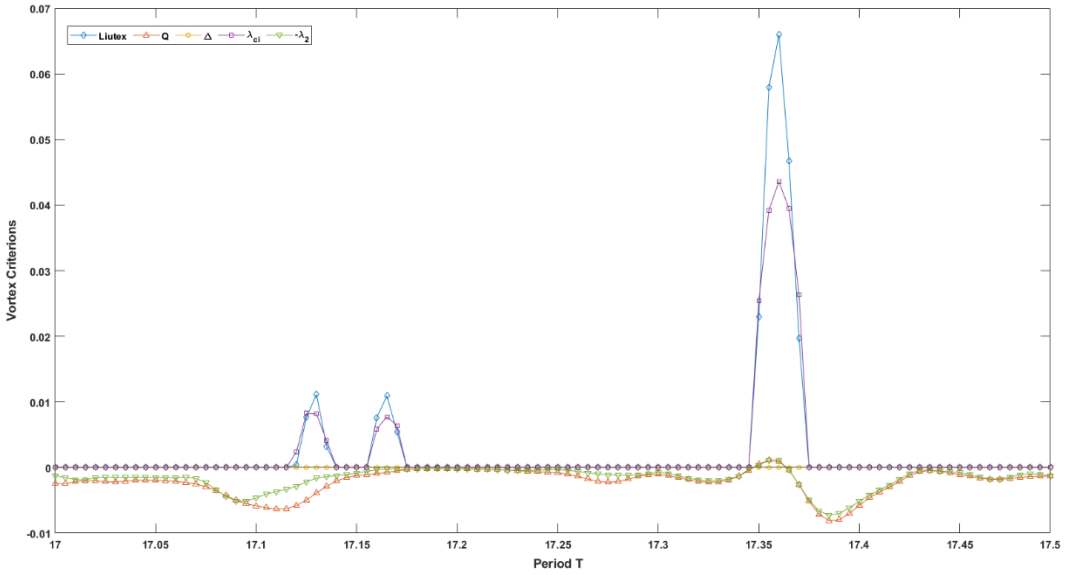

Fig. 5.7: Values of vortex criteria in different period T at x=500.7

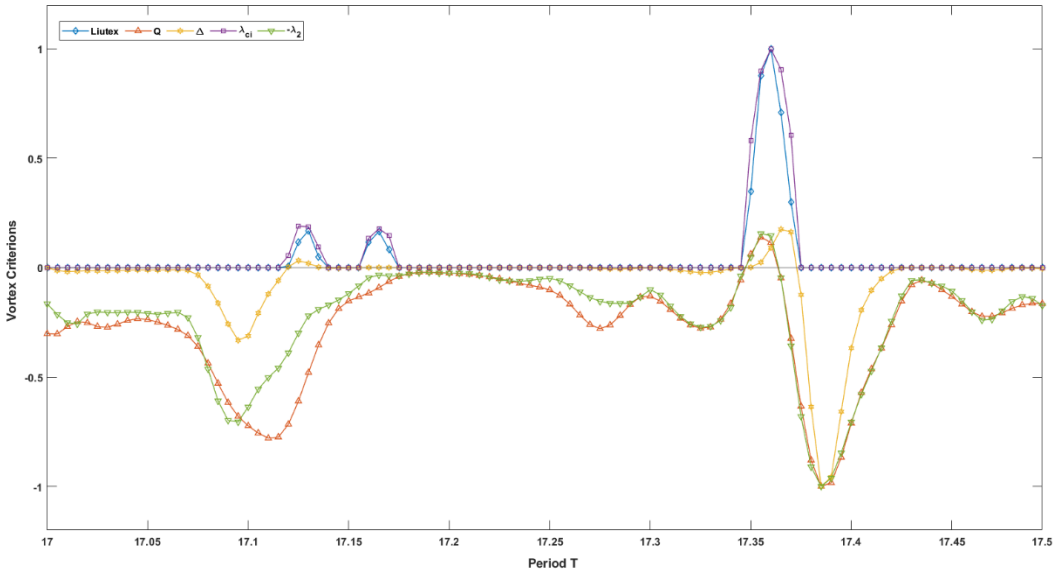

Fig. 5.8: Relative values of vortex criteria in different period T at x=500.7

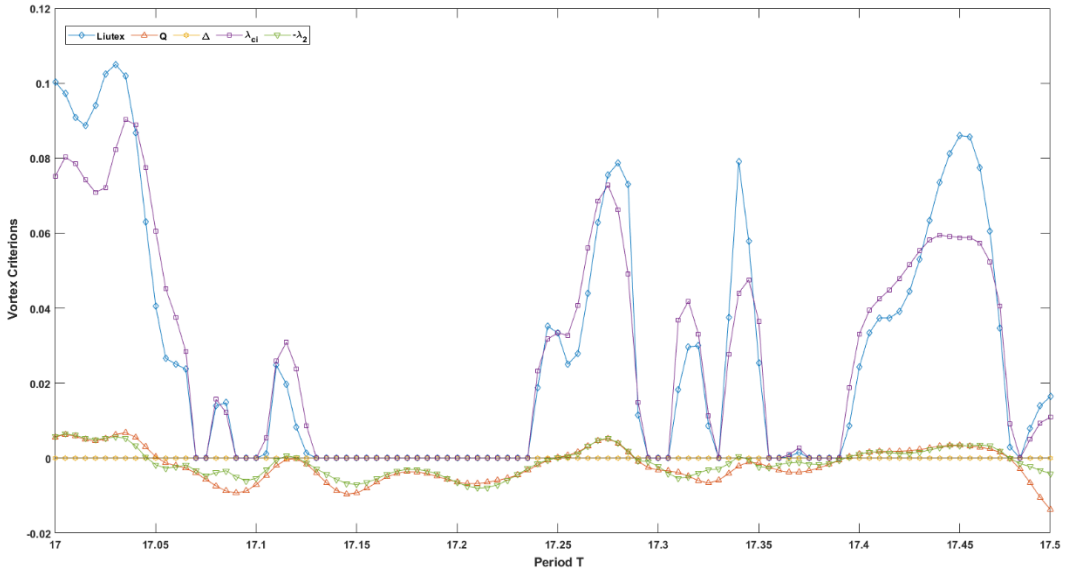

Fig. 5.9: Values of vortex criteria in different period T at x=815.5

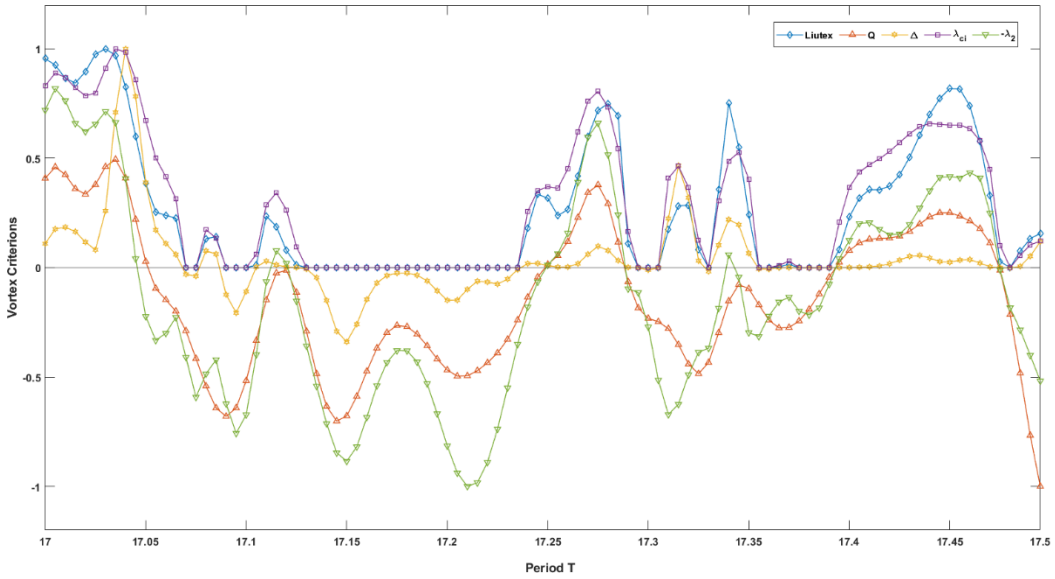

Fig. 5.10: Relative values of vortex criteria in different period T at x=815.5

In Fig. 5.5, the Q, λ_2, and Δ methods were closely wrapped around zero for period **T**. This indicates that the values of these methods were significantly minuscule in the laminar flow. On the other hand, λ_{ci}'s values followed the flow of Liutex, which is an indicator that λ_{ci}, and Liutex have

the same dimensional quantifier. In Fig. 5.6, the relative values reveal that Δ is positive when Liutex is positive. This satisfies the condition that a vortex region exists. However, we observed that Q and $-\lambda_2$ are not able to detect the weak vortex region.

In Fig. 5.7 and Fig. 5.9, the values of Q and $-\lambda_2$ in the transitional and turbulent flow were identical. This corresponds with the conclusions in graphical example 5.2.1 that their dimensions are the same. In Fig. 5.8 and Fig. 5.10, the relative values of Q and $-\lambda_2$ in the transitional and turbulent flow still had similar flow patterns but $-\lambda_2$ was able to detect some weak vortex regions that Q could not. In figures 5.7 to 5.10, the λ_{ci} method followed the flow of Liutex, again showing the close relationship between the two methods.

Based on the mathematical and graphical dimensional analysis, λ_{ci} seems to be the best method among the four second-generation vortex identification methods in comparison with Liutex.

5.3 Conclusion

The dimensional quantifier is very important because any mathematical equation relating physical quantities must be dimensionally consistent. Liutex magnitude R, equal to twice the angular velocity, has the same dimension as the angular velocity α. The dimensions of Q, λ_2, and Δ are not equivalent to the dimension of angular velocity α. Therefore, the values of Q, λ_2 and Δ can be significantly higher or lower than the value of α.

Only λ_{ci} had the proper dimensional quantifier to be comparable to Liutex magnitude R. Of the four second-generation methods, λ_{ci} is the only one not affected by stretching. However, λ_{ci} is affected by shear, is scalar-valued, and depends on a threshold to visualize the iso-surface. Therefore, Liutex is superior to the second-generation methods since it is defined as a vector, and Liutex magnitude R has the proper dimension.

Chapter 6

The Local Fluid Rotational Axis

6.1 Definition of the Local Fluid Rotational Axis

Definition 6.1:

The local fluid rotational axis is defined as a vector that can only have stretching (compressing) along its length and cannot rotate itself. In other words, the increment of velocity along the rotation axis $\vec{\gamma}$ must be along itself, i.e., $d\vec{\mathrm{v}} = c\vec{\gamma}$ (Liu et al. 2019, Gao et al. 2018).

From the definition of the velocity gradient tensor, $d\vec{v} = \mathbf{\nabla}\vec{\mathbf{v}} * \vec{\gamma}$. Therefore, $d\vec{\mathrm{v}} = \mathbf{\nabla}\vec{\mathbf{v}} * \vec{\gamma} = c\vec{\gamma}$ along the rotation axis. This indicates that $\vec{\gamma}$ is the real eigenvector of $\mathbf{\nabla}\vec{\mathbf{v}}$. Any axis that does not satisfy Definition 6.1 will not be a rotation axis.

6.2 Mathematical Analysis

There are five vector candidates for the local rotational axis. They are the symmetrical tensor's eigenvectors, the vorticity vector, and the Liutex directional unit vector.

6.2.1 Liutex directional vector

The definition of Liutex vector is $\vec{R} = R\vec{r}$, where $\vec{r}$ represents the directional unit vector of Liutex and is the real eigenvector of $\mathbf{\nabla}\vec{\mathbf{v}}$, i.e., $d\vec{v} = \mathbf{\nabla}\vec{\mathbf{v}} * \vec{r} = \lambda_r\vec{r}$. Therefore, the Liutex directional vector satisfies the definition of the local rotation axis.

Note: Since a normalized eigenvector is unique up to a $\pm$ sign, a second condition is imposed, which is $\vec{\omega} \cdot \vec{r} > 0$, where $\vec{\omega}$ is the vorticity vector.

6.2.2 The 3 Eigenvectors of the symmetrical tensor $\boldsymbol{A}$

The symmetrical tensor $\boldsymbol{A}$ in the principal coordinate is

$$\boldsymbol{A_\theta} = \begin{bmatrix} \lambda_{cr} & \frac{\varepsilon}{2} & \frac{\xi}{2} \\ \frac{\varepsilon}{2} & \lambda_{cr} & \frac{\eta}{2} \\ \frac{\xi}{2} & \frac{\eta}{2} & \lambda_r \end{bmatrix}. \tag{6.1}$$

Let λ_1, λ_2, and λ_3 be the eigenvalues of $\boldsymbol{A_\theta}$, and $\vec{d}_1$, $\vec{d}_2$ and $\vec{d}_3$ be the eigenvectors of $\boldsymbol{A_\theta}$,

i.e., $\vec{d}_i = [X_i \quad Y_i \quad Z_i]^T$, for $i = 1,2,3$.

Since $\boldsymbol{\nabla}\overrightarrow{\boldsymbol{V}_\theta} * \vec{\gamma} = d\vec{V} = c\vec{\gamma}$, then $\boldsymbol{\nabla}\overrightarrow{\boldsymbol{V}_\theta} * \vec{\gamma} = c\vec{\gamma}$.

Let $\vec{\gamma} = \vec{d}_i$, then,

$$\boldsymbol{\nabla}\overrightarrow{\boldsymbol{V}_\theta} * \vec{d}_i = \boldsymbol{A_\theta} * \vec{d}_i + \boldsymbol{B_\theta} * \vec{d}_i = \lambda_i \vec{d}_i + \boldsymbol{B_\theta} * \vec{d}_i$$

$$= \lambda_i \begin{bmatrix} X_i \\ Y_i \\ Z_i \end{bmatrix} + \begin{bmatrix} 0 & -\frac{R+\varepsilon}{2} & -\frac{\xi}{2} \\ \frac{R+\varepsilon}{2} & 0 & -\frac{\eta}{2} \\ \frac{\xi}{2} & \frac{\eta}{2} & 0 \end{bmatrix} \begin{bmatrix} X_i \\ Y_i \\ Z_i \end{bmatrix} = \lambda_i \begin{bmatrix} X_i \\ Y_i \\ Z_i \end{bmatrix} + \frac{1}{2} \begin{bmatrix} -(R+\varepsilon)Y_i - \xi Z_i \\ (R+\varepsilon)X_i - \eta Z_i \\ \xi X_i + \eta Y_i \end{bmatrix}$$

$$= \lambda_i \begin{bmatrix} X_i \\ Y_i \\ Z_i \end{bmatrix} + \left(- \begin{bmatrix} X_i \\ Y_i \\ Z_i \end{bmatrix} \times \begin{bmatrix} \eta \\ -\xi \\ R+\varepsilon \end{bmatrix} \right) = \lambda_i \vec{d}_i + \left(-\vec{d}_i \times \vec{\omega}\right) \neq c\vec{d}_i. \tag{6.2}$$

This implies that $\vec{d}_i$ does not satisfy the definition of the rotation axis. Therefore, the three eigenvectors of symmetrical tensor $\boldsymbol{A}$ are not the rotation axis. (Nottage et al. 2021)

6.2.3 The Vorticity Vector

The vorticity vector in the principal coordinates is

$$\boldsymbol{\nabla} \times \overrightarrow{\boldsymbol{V}_\theta} = \vec{\omega} = \begin{bmatrix} \eta \\ -\xi \\ R+\varepsilon \end{bmatrix}. \tag{6.3}$$

Since $\boldsymbol{\nabla}\overrightarrow{\boldsymbol{V}_\theta} * \vec{\gamma} = d\overrightarrow{\boldsymbol{V}_\theta} = c\vec{\gamma}$, then $\boldsymbol{\nabla}\overrightarrow{\boldsymbol{V}_\theta} * \vec{\gamma} = c\vec{\gamma}$ and let $\vec{\omega} = \vec{\gamma}$.

$$\boldsymbol{\nabla}\overrightarrow{\boldsymbol{V}_\theta} * \vec{\omega} = \boldsymbol{A_\theta} * \vec{\omega} + \boldsymbol{B_\theta} * \vec{\omega} = \boldsymbol{A_\theta} * \vec{\omega} + 0 = \begin{bmatrix} \lambda_{cr} & \frac{\varepsilon}{2} & \frac{\xi}{2} \\ \frac{\varepsilon}{2} & \lambda_{cr} & \frac{\eta}{2} \\ \frac{\xi}{2} & \frac{\eta}{2} & \lambda_r \end{bmatrix} \begin{bmatrix} \eta \\ -\xi \\ R+\varepsilon \end{bmatrix}$$

$$= \begin{bmatrix} \eta\lambda_{cr} \\ -\xi\lambda_{cr} \\ (R+\varepsilon)\lambda_r \end{bmatrix} + \frac{1}{2}\begin{bmatrix} R\xi \\ R\eta \\ 0 \end{bmatrix} = \lambda_{cr}\begin{bmatrix} \eta \\ -\xi \\ 0 \end{bmatrix} + \lambda_r\begin{bmatrix} 0 \\ 0 \\ (R+\varepsilon) \end{bmatrix} + \frac{R}{2}\begin{bmatrix} \xi \\ \eta \\ 0 \end{bmatrix} \tag{6.4}$$

Only in special cases does the equation stand:

$$\lambda_{cr}\begin{bmatrix} \eta \\ -\xi \\ 0 \end{bmatrix} + \lambda_r\begin{bmatrix} 0 \\ 0 \\ (R+\varepsilon) \end{bmatrix} + \frac{R}{2}\begin{bmatrix} \xi \\ \eta \\ 0 \end{bmatrix} = c\begin{bmatrix} \eta \\ -\xi \\ R+\varepsilon \end{bmatrix}. \tag{6.5}$$

The following are two cases where vorticity could possibly satisfy the equation above:

1) No rotation: If $\lambda_r = \lambda_{cr}$ and $R = 0$ then, (implies no rotation axis)

$$\lambda_{cr}\begin{bmatrix} \eta \\ -\xi \\ 0 \end{bmatrix} + \lambda_{cr}\begin{bmatrix} 0 \\ 0 \\ (0+\varepsilon) \end{bmatrix} + \frac{0}{2}\begin{bmatrix} \xi \\ \eta \\ 0 \end{bmatrix} = \lambda_{cr}\begin{bmatrix} \eta \\ -\xi \\ \varepsilon \end{bmatrix} = c\begin{bmatrix} \eta \\ -\xi \\ \varepsilon \end{bmatrix}. \tag{6.6}$$

2) No shear in the X and Y directions: If $\xi = \eta = 0$ then, (not possible in boundary layer)

$$\lambda_{cr}\begin{bmatrix} 0 \\ 0 \\ 0 \end{bmatrix} + \lambda_r\begin{bmatrix} 0 \\ 0 \\ (R+\varepsilon) \end{bmatrix} + \frac{R}{2}\begin{bmatrix} 0 \\ 0 \\ 0 \end{bmatrix} = \lambda_r\begin{bmatrix} 0 \\ 0 \\ (R+\varepsilon) \end{bmatrix} = c\begin{bmatrix} 0 \\ 0 \\ R+\varepsilon \end{bmatrix}. \tag{6.7}$$

This implies that the vorticity vector is not generally the rotation axis (Nottage et al. 2021).

6.3 Boundary Layer Transition DNS

A direct numerical simulation (DNS) is taken as an example to show the incorrectness mentioned above of the candidates (Nottage et al. 2021). The point selected to analyze is shown in Fig. 6.1.

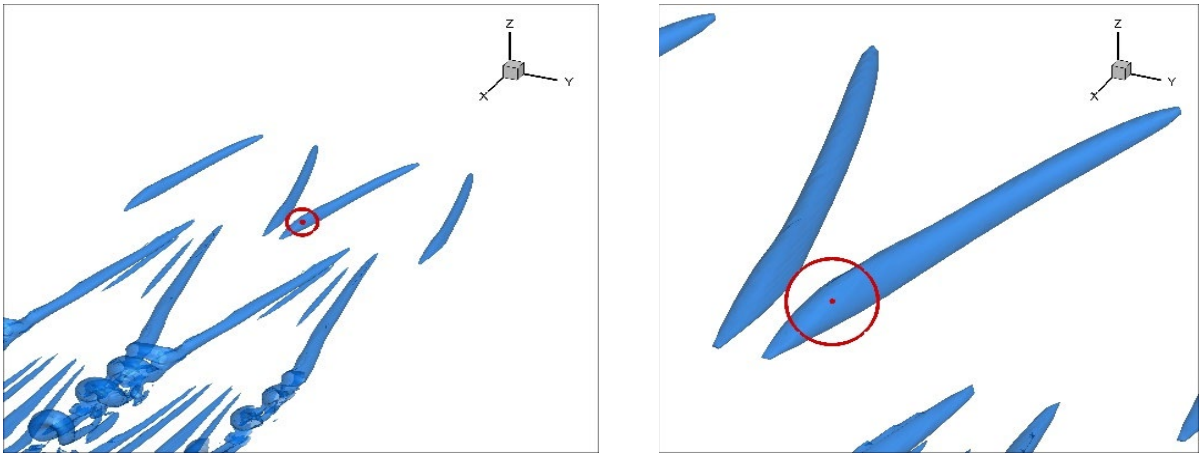

Fig. 6.1 The selected point

The velocity gradient tensor at this point is

$$\nabla\vec{\mathbf{v}} = \begin{bmatrix} 0.0533380 & 0.2818661 & 0.2621670 \\ -0.0139413 & 0.0003662 & 0.1193656 \\ -0.0055126 & -0.0798357 & -0.0548821 \end{bmatrix}. \tag{6.8}$$

The corresponding Liutex and vorticity can be expressed as:

$$\vec{R} = [-0.1292245 \quad 0.0197261 \quad -0.0100723]^T, \tag{6.9}$$

$$\vec{\omega} = [-0.1992013 \quad 0.2676797 \quad -0.2958074]^T. \tag{6.10}$$

The direction of the three eigenvectors of symmetric matrix $\boldsymbol{A}$ is:

$$\vec{d}_1 = [-0.6333458 \quad 0.4286110 \quad 0.6443335]^T, \tag{6.11}$$

$$\vec{d}_2 = [0.1600420 \quad -0.7420691 \quad 0.6509377]^T, \tag{6.12}$$

$$\vec{d}_3 = [0.7571391 \quad 0.5153891 \quad 0.4013906]^T. \tag{6.13}$$

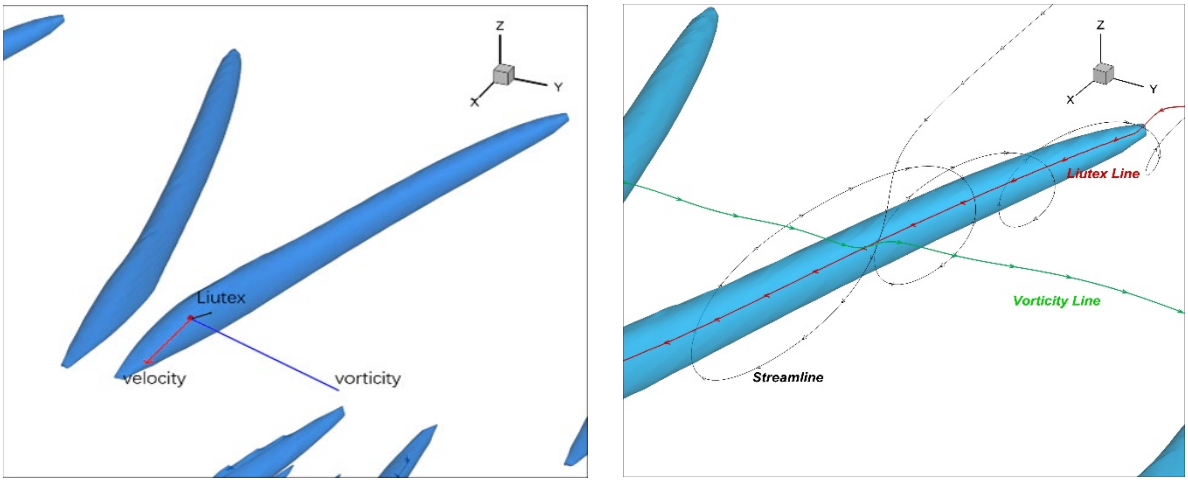

Fig. 6.2 Directions of Liutex, vorticity, and velocity

In Fig. 6.2, the Liutex line lies within the middle of the vortical structure, while the vorticity line is perpendicular to the vortical structure. Therefore, visually we can see that the vorticity vector is not the local fluid rotation axis. It is also worth noting that the streamlines are shown to swirl around the Liutex line. This is an indication that the Liutex directional vector is the local fluid rotation axis.

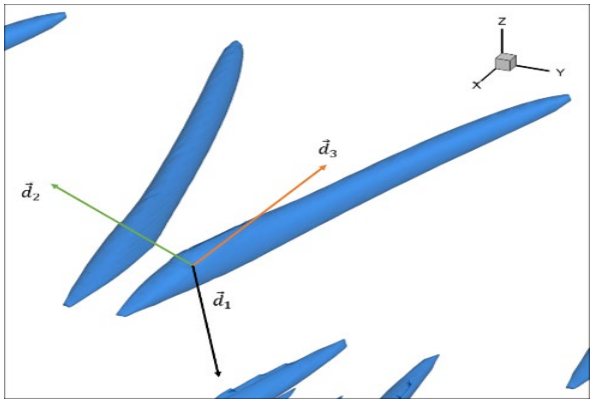

Fig. 6.3 Directions of the three eigenvectors of the symmetric matrix *A*

In Fig. 6.3, the directions of three eigenvectors of the symmetric matrix *A* are shown. All of them stretch in different directions, and none of them are aligned with the vortical structure.

6.3.1 Testing condition 1

Condition 1: The rotation axis can only be stretched or compressed in one of the physical rotation instances.

The increase of velocity along Liutex, vorticity, and the eigenvectors are described as follows:

$$d\vec{\mathbf{v}}_R = \nabla\vec{\mathbf{v}} * \vec{R} = [-0.0039731 \quad 6.0649258 \quad -3.0968137]^T, \tag{6.14}$$

$$d\vec{\mathbf{v}}_\omega = \nabla\vec{\mathbf{v}} * \vec{\omega} = [0.0127261 \quad -0.0324341 \quad -0.0040377]^T, \tag{6.15}$$

$$d\vec{\mathbf{v}}_{d1} = \nabla\vec{\mathbf{v}} * \vec{d}_1 = [0.2559524 \quad 0.0858979 \quad -0.0660894]^T, \tag{6.16}$$

$$d\vec{\mathbf{v}}_{d2} = \nabla\vec{\mathbf{v}} * \vec{d}_2 = [-0.0299734 \quad 0.0751966 \quad 0.0226365]^T, \tag{6.17}$$

$$d\vec{\mathbf{v}}_{d3} = \nabla\vec{\mathbf{v}} * \vec{d}_3 = [0.2908864 \quad 0.0375455 \quad -0.0673495]^T. \tag{6.18}$$

The vectors are normalized to avoid the influence of magnitudes.

To test if the directions of two vectors are parallel, the cross-product result is used:

$$(d\vec{\mathbf{v}}_R)_{normed} \times \vec{R}_{normed} = [-3.5 \times 10^{-18} \quad 2.5 \times 10^{-17} \quad 1.1 \times 10^{-16}]^T \approx \vec{0}, \tag{6.19}$$

$$(d\vec{\mathbf{v}}_\omega)_{normed} \times \vec{\omega}_{normed} = [0.68 \quad -0.19 \quad -0.63]^T \neq \vec{0}, \tag{6.20}$$

$$\left(d\vec{\mathbf{v}}_{d_1}\right)_{normed} \times \vec{d}_{1_{normed}} = [0.08 \quad -0.12 \quad 0.16]^T \neq \vec{0}, \tag{6.21}$$

$$\left(d\vec{\mathbf{v}}_{d_2}\right)_{normed} \times \vec{d}_{2_{normed}} = [0.07 \quad 0.02 \quad 0.01]^T \neq \vec{0}, \tag{6.22}$$

$$\left(d\vec{\mathbf{v}}_{d_3}\right)_{normed} \times \vec{d}_{3_{normed}} = [0.05 \quad -0.17 \quad 0.12]^T \neq \vec{0}. \tag{6.23}$$

If two vectors are parallel, then their cross-product equals the zero vector. Based on the calculation above, only the cross-product with Liutex was approximately the zero vector. Therefore, only Liutex satisfies the first condition of the rotation axis (Nottage et al. 2021).

6.3.2 Testing condition 2

Condition 2: The rotation axis cannot rotate itself.

In classical theory, the vorticity tensor is misunderstood to represent the rotation part; however, the real rotation part should be described by Liutex. The rotation matrix D is:

$$D = \begin{bmatrix} 0 & -\frac{1}{2}R_z & \frac{1}{2}R_y \\ \frac{1}{2}R_z & 0 & -\frac{1}{2}R_x \\ -\frac{1}{2}R_y & \frac{1}{2}R_x & 0 \end{bmatrix} = \begin{bmatrix} 0 & 0.0050362 & 0.0098630 \\ -0.0050362 & 0 & 0.0646122 \\ -0.0098630 & -0.0646122 & 0 \end{bmatrix}. \quad (6.24)$$

To test if the vectors rotate themselves, the multiplication between D and the normalized vectors is calculated:

$$D * \vec{R}_{normed} = [0 \quad 0 \quad 0]^T, \quad (6.25)$$

$$D * \vec{\omega}_{normed} = [-0.0035 \quad -0.0406 \quad -0.0344]^T, \quad (6.26)$$

$$D * \vec{d}_{1_{normed}} = [0.0085 \quad 0.0448 \quad -0.0214]^T, \quad (6.27)$$

$$D * \vec{d}_{2_{normed}} = [0.0027 \quad 0.0413 \quad 0.0464]^T, \quad (6.28)$$

$$D * \vec{d}_{3_{normed}} = [0.0066 \quad 0.0221 \quad -0.0408]^T. \quad (6.29)$$

If the multiplication is equal to the zero vector, the candidate vector is not rotated. Based on the calculation above, only the dot product with Liutex is equal to the zero vector. Therefore, Liutex is the only one that satisfies the second condition of the rotation axis (Nottage et al. 2021).

6.4 Conclusion

The local rotational axis is defined as a vector along which the velocity increment can only have stretching (compression) along its length (Definition 6.1). Vorticity vector is, in general, not the rotation axis, which directly opposes the traditional and classical concepts in fluid kinematics. Vorticity vector is rotation axis only when shear is zero, which cannot occur in boundary layers.

The direction of vorticity was misunderstood as the rotational axis because people incorrectly considered matrix $\boldsymbol{A}$ as stretching and antisymmetric matrix $\boldsymbol{B}$ as rotation. Liutex is the only candidate for the local rotation axis as it satisfies Definition 6.1.

Chapter 7
Vorticity is not vortex

7.1 Vorticity = rotation + shear

In Computational fluid dynamics, many researchers and textbooks accept that vorticity is vortex. This is due to a misunderstanding from the Cauchy-Stokes decomposition of velocity gradient tensor. It was understood that the symmetric tensor $\boldsymbol{A}$ represented stretching/compression, and the antisymmetric tensor $\boldsymbol{B}$ (vorticity tensor) represented rotation. In this section, I will prove and give evidence to back up my claim that vorticity is not vortex as it consists of rotation and shear components.

7.1.1 Vorticity tensor in the Principal Coordinate

$$\boldsymbol{B_\theta} = \begin{bmatrix} 0 & \frac{1}{2}\left(\frac{\partial U}{\partial Y} - \frac{\partial V}{\partial X}\right) & \frac{1}{2}\left(\frac{\partial U}{\partial Z} - \frac{\partial W}{\partial X}\right) \\ \frac{1}{2}\left(\frac{\partial V}{\partial X} - \frac{\partial U}{\partial Y}\right) & 0 & \frac{1}{2}\left(\frac{\partial V}{\partial Z} - \frac{\partial W}{\partial Y}\right) \\ \frac{1}{2}\left(\frac{\partial W}{\partial X} - \frac{\partial U}{\partial Z}\right) & \frac{1}{2}\left(\frac{\partial W}{\partial Y} - \frac{\partial V}{\partial Z}\right) & 0 \end{bmatrix} = \begin{bmatrix} 0 & -\frac{R+\varepsilon}{2} & -\frac{\xi}{2} \\ \frac{R+\varepsilon}{2} & 0 & -\frac{\eta}{2} \\ \frac{\xi}{2} & \frac{\eta}{2} & 0 \end{bmatrix}$$

$$= \begin{bmatrix} 0 & -\frac{R}{2} & 0 \\ \frac{R}{2} & 0 & 0 \\ 0 & 0 & 0 \end{bmatrix} + \begin{bmatrix} 0 & -\frac{\varepsilon}{2} & -\frac{\xi}{2} \\ \frac{\varepsilon}{2} & 0 & -\frac{\eta}{2} \\ \frac{\xi}{2} & \frac{\eta}{2} & 0 \end{bmatrix} = \boldsymbol{R} + \boldsymbol{AS}. \tag{7.1}$$

Therefore, $\boldsymbol{B_\theta}$ (vorticity tensor) can be decomposed further to yield $\boldsymbol{R}$ (rotation part or Liutex) and $\boldsymbol{AS}$ (the antisymmetric shear deformation part). This decomposition implies that the vorticity tensor is not strictly rotation (Yu et al. 2020).

7.1.2 Vorticity vector in the Principal Coordinate

7.1.2.1 Proof 1

$$\overrightarrow{\omega} = \boldsymbol{\nabla} \times \overrightarrow{\boldsymbol{V_\theta}} = \left(\frac{\partial}{\partial X}, \frac{\partial}{\partial Y}, \frac{\partial}{\partial Z}\right)^{\boldsymbol{T}} \times (U, V, W)^{\boldsymbol{T}} = \left(\frac{\partial W}{\partial Y} - \frac{\partial V}{\partial Z}, \frac{\partial U}{\partial Z} - \frac{\partial W}{\partial X}, \frac{\partial V}{\partial X} - \frac{\partial U}{\partial Y}\right)^{\boldsymbol{T}}$$

$$= \left(\eta, -\xi, \frac{R}{2} + \varepsilon - \left(-\frac{R}{2}\right)\right)^{\boldsymbol{T}} = (\eta, -\xi, R + \varepsilon)^{\boldsymbol{T}}$$

$$= (\eta, -\xi, \varepsilon)^{\boldsymbol{T}} + (0, 0, R)^{\boldsymbol{T}} = \vec{S} + \vec{R} \tag{7.2}$$

Therefore, $\overrightarrow{\omega}$ contains shearing and rotation components (Shrestha et al. 2021).

7.1.2.2 Proof 2

Let $d\vec{c}$ be an arbitrarily selected real vector, $d\vec{c} = \begin{bmatrix} \dot{x} \\ \dot{y} \\ \dot{z} \end{bmatrix}$.

$$2\boldsymbol{B_\theta} * d\vec{c} = 2\begin{bmatrix} 0 & -\frac{R+\varepsilon}{2} & -\frac{\xi}{2} \\ \frac{R+\varepsilon}{2} & 0 & -\frac{\eta}{2} \\ \frac{\xi}{2} & \frac{\eta}{2} & 0 \end{bmatrix}\begin{bmatrix} \dot{x} \\ \dot{y} \\ \dot{z} \end{bmatrix} = \begin{bmatrix} -(R+\varepsilon)\dot{y} - \xi\dot{z} \\ (R+\varepsilon)\dot{x} - \eta\dot{z} \\ \xi\dot{x} + \eta\dot{y} \end{bmatrix}$$

$$= -\begin{bmatrix} \dot{x} \\ \dot{y} \\ \dot{z} \end{bmatrix} \times \begin{bmatrix} \eta \\ -\xi \\ R+\varepsilon \end{bmatrix} = -d\vec{c} \times \left(\boldsymbol{\nabla} \times \overrightarrow{\boldsymbol{V_\theta}}\right). \tag{7.3}$$

$$2\boldsymbol{B_\theta} * d\vec{c} = (2\boldsymbol{R} + 2\boldsymbol{AS}) * d\vec{c} = 2\boldsymbol{R} * d\vec{c} + 2\boldsymbol{AS} * d\vec{c}$$

$$= \begin{bmatrix} 0 & -R & 0 \\ R & 0 & 0 \\ 0 & 0 & 0 \end{bmatrix}\begin{bmatrix} \dot{x} \\ \dot{y} \\ \dot{z} \end{bmatrix} + \begin{bmatrix} 0 & -\varepsilon & -\xi \\ \varepsilon & 0 & -\eta \\ \xi & \eta & 0 \end{bmatrix}\begin{bmatrix} \dot{x} \\ \dot{y} \\ \dot{z} \end{bmatrix} = \begin{bmatrix} -R\dot{y} \\ R\dot{x} \\ 0 \end{bmatrix} + \begin{bmatrix} -\varepsilon\dot{y} - \xi\dot{z} \\ \varepsilon\dot{x} - \eta\dot{z} \\ \xi\dot{x} + \eta\dot{y} \end{bmatrix}$$

$$= -\begin{bmatrix} \dot{x} \\ \dot{y} \\ \dot{z} \end{bmatrix} \times \begin{bmatrix} 0 \\ 0 \\ R \end{bmatrix} - \begin{bmatrix} \dot{x} \\ \dot{y} \\ \dot{z} \end{bmatrix} \times \begin{bmatrix} \eta \\ -\xi \\ \varepsilon \end{bmatrix} = -d\vec{c} \times \vec{R} - d\vec{c} \times \vec{S}. \tag{7.4}$$

$$\Longrightarrow \quad -d\vec{c} \times \vec{R} - d\vec{c} \times \vec{S} = \boldsymbol{2B_\theta} * d\vec{c} = -d\vec{c} \times \left(\boldsymbol{\nabla} \times \overrightarrow{\boldsymbol{V_\theta}}\right) \tag{7.5}$$

$$\Longrightarrow \quad d\vec{c} \times \left(\boldsymbol{\nabla} \times \overrightarrow{\boldsymbol{V_\theta}}\right) = d\vec{c} \times \vec{R} + d\vec{c} \times \vec{S} = d\vec{c} \times \left(\vec{R} + \vec{S}\right) \tag{7.6}$$

Since $d\vec{c}$ was arbitrarily selected, then, $\boldsymbol{\nabla} \times \overrightarrow{\boldsymbol{V_\theta}} = \vec{R} + \vec{S}$, where $\vec{R}$ is a rotational vector and $\vec{S}$ is a

non-rotational shear vector. 7.1.2.1 and 7.1.2.2 imply that the vorticity vector contains rotational and shearing factors; hence the vorticity vector is not strictly rotational (Jeong et al. 1995, Nottage et al. 2021).

7.1.3 Vorticity Magnitude in the Principal Coordinate

The vorticity magnitude in the Principal Coordinate is $\|\vec{\omega}\| = \sqrt{(\eta)^2 + (\xi)^2 + (R + \varepsilon)^2}$.

The vorticity magnitude contains rotation R and shearing components η, ξ, ε (Shrestha et al. 2021).

7.2 Statistical analysis of vorticity (ω), Liutex (l), and shear (s).

Using a direct numerical simulation (DNS), we will:

1) Investigate the behavior of shear, Liutex, and vorticity from laminar flow to turbulent flow.
2) Analyze the effect of shear on vorticity.

The results of the DNS over a grid of $1920 \times 128 \times 241$ are recorded.

Statistical analysis is performed over the whole grid domain and across 500 t time steps.

The Statistical integration formula is $\sum_i \sum_j \sum_k \tau_{ijkt} vol_{ijk} = \iota_t$, where τ_{ijkt} is a point in the grid, i = 1 to 1920, j = 1 to 128, k = 1 to 241 and t represents the step-in time. vol_{ijk} is the volume of the space around the point τ_{ijkt}. ι_t is the integration output value in time t. We calculate and record the data across time t = 10 to 15 for:

- l_{mag} = Liutex magnitude component
- ω_{mag} = vorticity magnitude component
- s_{mag} = shear magnitude component
- l_y = Liutex component in the y direction

- ω_y = vorticity component in the y direction
- s_y = shear component in the y direction

The difference in the values of vorticity and Liutex is significantly high, so the relative values are used to compare the change in the values over period T.

7.2.1 Whole domain for the y direction

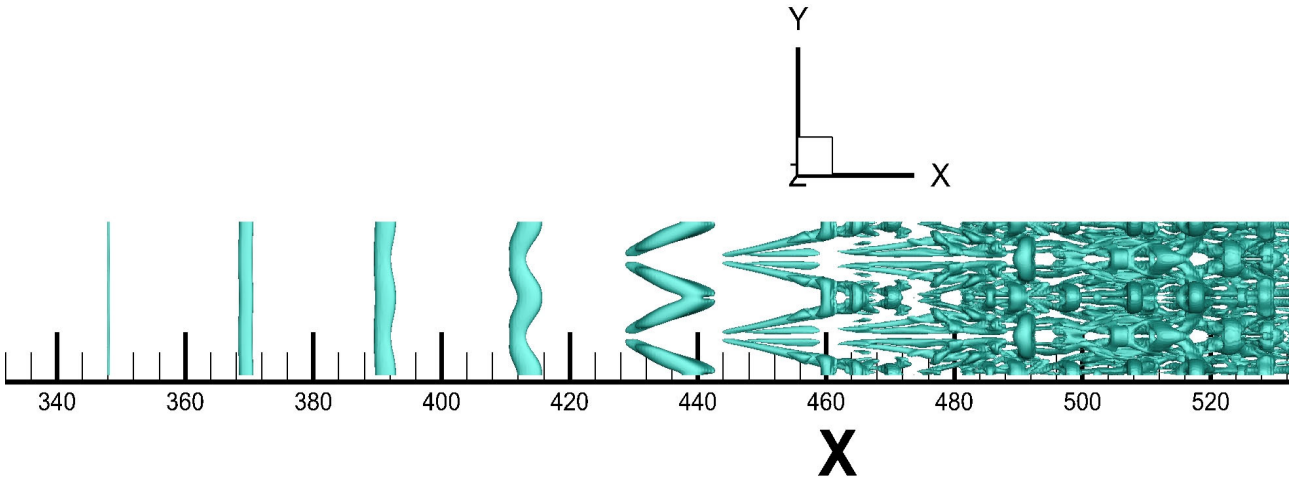

Fig. 7.1: Vortex structures by modified Liutex-Omega with $\widetilde{\Omega}_L = 0.52$ at t = 13.00T

Figure 7.1 shows the formation of the vortex structures from the Y direction view in laminar flow from 340 to 400, transitional flow from 401 to 470, and turbulent flow from 471 to 520. In laminar flow, there is no vortex structure. In transition flow, the formation of hairpin vortex rings begins, and in turbulent flow, many vortex rings have formed.

The spanwise Y direction is the most prominent since it contributes the most to the value of the magnitudes (Dong et al. 2018).

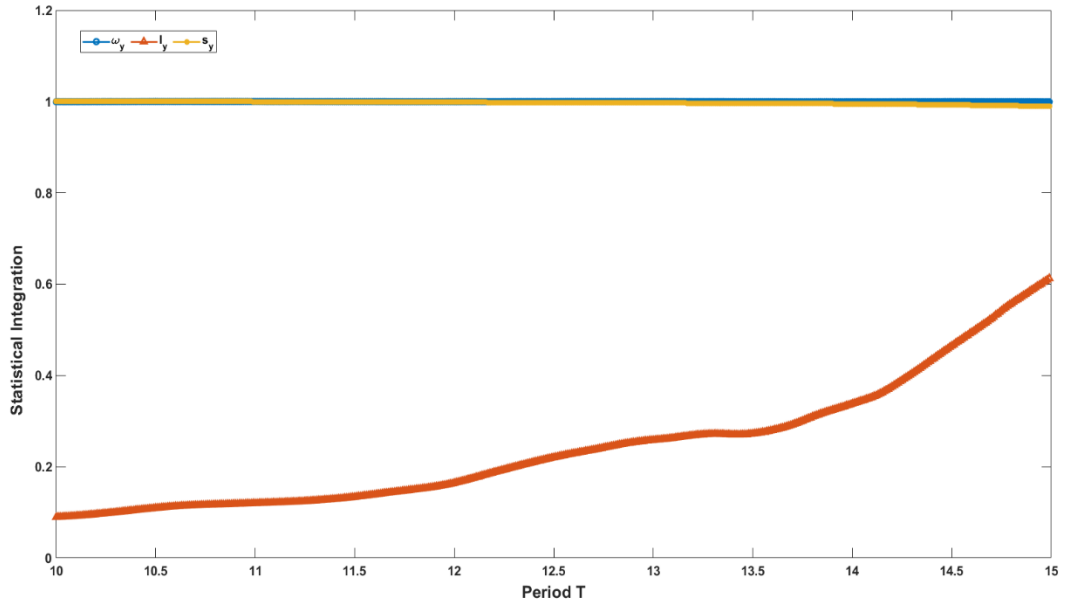

Fig. 7.2: Relative integration values for ω_y, l_y & s_y from T = 10 to 15

In Fig. 7.2, the relative $\boldsymbol{l_y}$ values increased significantly over period **T**, which is the T-S wave period. $\boldsymbol{\omega_y}$ showed no change throughout period **T**. The change in $\boldsymbol{s_y}$ values were negative, which coincides with the increase in $\boldsymbol{l_y}$ and no change in $\boldsymbol{\omega_y}$. The period **T** travels from laminar flow to turbulent flow. There should be minuscule rotation or vortex activity in laminar flow, and then as we move into transitional flow, the vortex activity increases, creating hairpin vortex rings. This coincides with $\boldsymbol{l_y}$ relative values behavior.

7.2.2 Whole domain for magnitudes

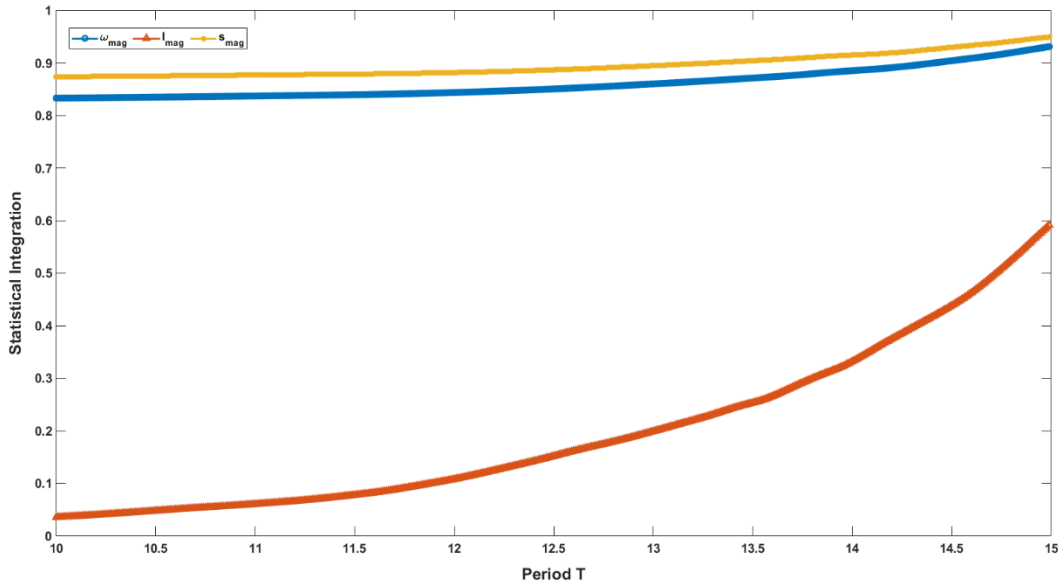

Fig. 7.3: Relative Integration values for ω_{mag}, l_{mag} & s_{mag} from T = 10 to 15

It can be observed from Fig. 7.3 that the relative change in $\boldsymbol{l_{mag}}$ across time is much greater than $\boldsymbol{\omega_{mag}}$. As we moved from laminar flow to turbulent flow in time, the values of $\boldsymbol{l_{mag}}$ continually increased, showing that $\boldsymbol{l_{mag}}$ picked up the formation of vortex rings, whereas $\boldsymbol{\omega_{mag}}$ barely changed.

7.3 Conclusion

Vorticity is not strictly rotation since shear contaminates it. The effect of shear on vorticity can substantially lead to a misrepresentation of vortex indication in the laminar flow with no rotation. The Y direction relative graph shows that over time $\boldsymbol{\omega_y}$ had little to no change in value, while $\boldsymbol{l_y}$ increased as time progressed. This occurs because the hairpin vortex rings form in the Y direction during transitional flow. However, since $\boldsymbol{\omega_y}$ had little to no change throughout period **T**, it cannot identify the formation of these hairpin vortex rings.

Since the $\boldsymbol{\omega_y}$ change in values was minuscule but $\boldsymbol{l_y}$ values were increasing, $\boldsymbol{s_y}$ values were decreasing. Therefore, Liutex has a negative relation with shear deformation. The magnitude graphs show that the relative increase in $\boldsymbol{l_{mag}}$ as time progressed was more significant than the increase in $\boldsymbol{\omega_{mag}}$ and $\boldsymbol{s_{mag}}$. Since vorticity misrepresented shear as rotation in laminar flow and could not identify when the hairpin vortex rings formed, vorticity should not be considered as vortex.

Summary of the Conclusions

In Chapter 5, the importance of the dimensional quantifier was emphasized. Any mathematical equation relating physical quantities must be dimensionally consistent. Liutex magnitude R, equal to twice the angular velocity, has the same dimension as the angular velocity α. The dimensions of Q, λ_2, and Δ are not equivalent to the dimension of angular velocity α. Therefore, the values of Q, λ_2 and Δ can be significantly higher or lower than the value of α. Only λ_{ci} had the proper dimensional quantifier to be comparable to Liutex magnitude R. Of the four second-generation methods, λ_{ci} is the only one not affected by stretching. However, λ_{ci} is affected by shear, is scalar-valued, and depends on a threshold to visualize the iso-surface. Therefore, Liutex is superior to the second-generation methods since it is defined as a vector, and its magnitude R has the proper dimension.

In Chapter 6, the local rotational axis was defined. Five vector candidates were assessed to find the proper vector that can represent the local rotational axis. The local rotational axis is defined as a vector along which the velocity increment can only have stretching (compression) along its length (Definition 6.1). The eigenvectors of the symmetric tensor $\boldsymbol{A}$ failed to satisfy definition 6.1. The vorticity vector, in general, is not the rotation axis, which directly opposes the traditional and classical concepts in fluid kinematics. The vorticity vector is rotation axis only when shear is zero, which cannot occur in boundary layers. The direction of vorticity was misunderstood as the rotational axis because people incorrectly considered matrix $\boldsymbol{A}$ as stretching and antisymmetric matrix $\boldsymbol{B}$ as rotation. Liutex is the only candidate for the local rotation axis as it satisfies Definition 6.1.

Lastly, in chapter 7, the relationship and behavior of vorticity, Liutex, and shear were observed over period **T** (10 to 15). Vorticity was proven to be contaminated by shear and is not strictly rotation.

The effect of shear on vorticity can be very significant, which leads to a misrepresentation of vortex indication in the laminar flow where there is no rotation. The Y direction relative graph showed that over time $\boldsymbol{\omega_y}$ had little to no change in value, while $\boldsymbol{l_y}$ increased as time progressed. This occurred because the hairpin vortex rings form in the Y direction during transitional flow. Since $\boldsymbol{\omega_y}$ had little to no change throughout period **T**, it cannot identify the formation of these hairpin vortex rings.

Since the $\boldsymbol{\omega_y}$ change in values was minuscule, but $\boldsymbol{l_y}$ values increased significantly, the $\boldsymbol{s_y}$ values decreased. Therefore, Liutex has a negative relation with shear deformation. Since vorticity misrepresented shear as rotation in laminar flow and could not identify when the hairpin vortex rings formed, vorticity should not be considered as vortex.

Bibliography

Chakraborty, P., Balachandar, S., & Adrian, R. (2005). On the relationships between local vortex identification schemes. *Journal of Fluid Mechanics, 535*, 189-214.

Chong, M. S., & Perry, A. E. (1990). A general classification of three-dimensional flow fields. *Physics of Fluids A: Fluid Dynamics, 2*(5), 765-777. doi:https://doi.org/10.1063/1.857730

Dong, X., Tian, S., & Liu, C. (2018). Correlation analysis on volume vorticity and vortex in late boundary layer transition. *Physics of Fluids, 30*(1), 014105. doi:https://doi.org/10.1063/1.5009115

Dong, X.-r., Wang, Y.-q., Chen, X.-p., Dong, Y., Zhang, Y.-n., & Liu, C. (2018). Determination of epsilon for Omega vortex identification method. *Journal of Hydrodynamics, 30*(4), 541-548. doi:https://doi.org/10.1007/s42241-018-0066-x

Epps, B. (2017). Review of Vortex Identification Methods. Grapevine, Texas, USA: 55th AIAA Aerospace Sciences Meeting. doi:https://doi.org/10.2514/6.2017-0989

Gao, Y., & Liu, C. (2018). Rortex and comparison with eigenvalue-based vortex identification criteria. *Physics of Fluids, 30*(8), 085107.

Gao, Y., Liu, J., Yu, Y., & Liu, C. (2019). A Liutex based definition and identification of vortex core center lines. *Journal of Hydrodynamics, 31*(3), 445-454.

Haller, G. (2005). An Objective definition of a Vortex. *Journal of Fluid Mechanics, 525*, 1-26. doi:https://doi.org/10.1017/s0022112004002526

Helmholtz, H. (1858). On the integrals of the hydrodynamic equations corresponding to vortex motions. *Journal für die reine und angewandte Mathematik (Crelles Journal), 55*, 22-25.

Hunt, J., Wray, A., & Moin, P. (1988). Eddies, stream, and convergence zones in turbulent flows. *Center for Turbulent Research*, (pp. 193-208).

Jeong, J., & Hussain, F. (1995). On the identification of a vortex. *Journal of Fluid Mechanics, 285*, 69-94. doi:10.1017/s0022112095000462

Liu, C., Gao, Y., Tian, S., & Dong, X. (2018). Rortex - A new vortex vector definition and vorticity tensor and vector decompositions. *Physics of Fluids, 30*(3). doi:https://doi.org/10.1063/1.5023001

Liu, C., Gao, Y.-s., Dong, X.-r., Wang, Y.-q., Liu, J.-m., Zhang, Y.-n., . . . Gui, N. (2019). Third generation of vortex identification methods: Omega and Liutex/Rortex Based systems. *Journal of Hydrodynamics, 31*, 205-223. doi:https://doi.org/10.1007/s42241-019-0022-4

Liu, C., Wang, Y., Yang, Y., & Duan, Z. (2016). New omega vortex identification method. *Science China Physics, Mechanics & Astronomy, 59*(8), 684711.

Liu, C., Yan, Y., Tian, S., & Dong, X. (2018). Rortex- a new vortex vector definition and Vorticity

tensor and vector decompositions. *Physics of Fluids, 30*(3), 035103.

Liu, C., Yun, Y., & Lu, P. (2014). Physics of turbulence generation and sustenance in a boundary layer. *Computer & Fluids, 102*, 353-384.

Liu, J., Wang, Y., Gao, Y., & Liu, C. (2019). Galilean invariance of Omega vortex identification method. *Journal of Hydrodynamics, 31*, 249-255.

Moebs, W., Ling, S., & Sanny, J. (2016). *University Physics (Vol. 1).* Retrieved from OpenStax: https://openstax.org/books/university-physics-volume-1

Nottage, C., Yu, Y., & Liu, C. (2021). Mathematical Study on Local Fluid Rotation Axis: Vorticity is Not the Rotation Axis. In C. Liu, & Y. Wang (Eds.), *Liutex and Third Generation of Vortex Definition and Identification* (pp. 71-84). Springer, Cham.

Nottage, C., Yu, Y., Shrestha, P., & Liu, C. (2021). Dimensional and Theoretical Analysis of Second-Generation Vortex Identification Methods. In C. Liu, & Y. Wang (Eds.), *Liutex and Third Generation of Vortex Definition and Identification* (pp. 57-70). Springer, Cham.

Perry, A., & Chong, M. (1987). A Description of eddying motions and flow patterns using critical-point concepts. *Annual Review of Fluid Mechanics, 19*(1), 125-155.

Robinson, S. (1991). Coherent motions in turbulent boundary layer. *Annual Review of Fluid Mechanics, 23*, 601-639.

Saffman, P. (1993). *Vortex Dynamics.* Cambridge University Press.

Shrestha, P., Nottage, C., & Yu, Y. (2021). Stretching and shearing contamination analysis for Liutex and other vortex identification methods. *Advances in Aerodynamics, 3*(8).

Wang, J., Gao, Y., & Liu, C. (2019). Explicit formula for the Liutex vector and physical meaning of Vorticity based on the Liutex-Shear decomposition. *Journal of Hydrodynamics, 31*(3), 464-474.

Wang, Y., Gao, Y., & Liu, C. (2018). Galilean invariance of Rortex. *Physics of Fluids, 30*(11), 111701.

Wang, Y., Yang, Y., Yang, G., & Liu, C. (2017). DNS study on vortex and vorticity in late boundary layer transition. *Communications in Computational Physics, 22*(2), 441-459.

Wu, X., & Moin, P. (2009). Direct numerical simulation of turbulence in a nominally zero-pressure-gradient flat-plate boundary layer. *Journal of Fluid Mechanics, 630*, 5-41.

Yan, Y., Chen, C., Huankun, F., & Liu, C. (2014). DNS study on Λ-vortex and vortex ring formation in the flow transition at Mach number 0.5. *Journal of Turbulence, 15*(1), 1-21.

Yu, Y., Shrestha, P., Alvarez, O., Nottage, C., & Liu, C. (2020). Correlation analysis among vorticity, Q, and Liutex. *Journal of Hydrodynamics, 32*, 1207-1211.

Yu, Y., Shrestha, P., Alvarez, O., Nottage, C., & Liu, C. (2021). Investigation of correlation

between vorticity, Q, λ_ci, λ_2, Δ, and Liutex. *Computers & Fluids, 225*, 104977.

Yu, Y., Shrestha, P., Nottage, C., & Liu, C. (2020). Principal coordinates and principal velocity gradient tensor decomposition. *Journal of Hydrodynamics, 32*, 441-453.

Zhang, Y., Liu, K., Li, J., Xian, H., & Du, X. (2018). Analysis of the vortices in the inner flow of reversible pump-turbine with the new omega vortex identification method. *Journal of Hydrodynamics, 30*(3), 463-469.

Zhou, J., Adrian, R., Balachandar, S., & Kendall, T. (1999). Mechanisms for generating coherent packets of hairpin vortices in channel flow. *Journal of Fluid Mechanics, 387*, 353-396.

Zhou, Y., & Antonia, R. (1993). A study of turbulent vortices in the near wake of a cylinder. *Journal of Fluid Mechanics, 253*, 643-661.

Biographical Statement

Charles Matthew Nehemiah Nottage was born in Nassau, The Bahamas. He earned his Bachelor of Science degree in Mathematics from the University of the Bahamas (formerly known as The College of the Bahamas) in December 2011. He started the BS to Ph.D. track in Mathematics at The University of Texas at Arlington in January 2013. In May 2017, he completed all requirements to earn his Master of Science degree. In 2016, he joined Dr. Chaoqun Liu's research group, where he learned about Computational Fluid Dynamics. In June 2020, the 13th International Academic Conference Chaos 2020 was held virtually, where he participated as a presenter and a session chair for the Liutex workshop. In 2020-2021, he co-authored four published journal articles and three book chapters in Liutex and Third Generation of Vortex Definition and Identification. He is currently working on publishing three journal papers as the first author. He was inducted into the National Society of Leadership and Success (ΣΑΠ) in 2010 and Pi Mu Epsilon in May 2018.